A unified rodent atlas reveals the cellular complexity and evolutionary divergence of the dorsal vagal complex

Cecilia Hes[a,b], Abigail J. Tomlinson[c], Lieke Michielsen[d], Hunter J. Murdoch[a,e], Fatemeh Soltani[a,b], Maia Kokoeva[a,e,f], Paul V. Sabatini[a,b,e,f]

[a] Research Institute of the McGill University Health Centre, McGill University Health Centre, 1001 boulevard de Decarie, Montreal, Quebec H4A 3J1, Canada.

[b] Division of Experimental Medicine, Department of Medicine, McGill University, 1001 boulevard de Decarie, Montreal, Quebec H4A 3J1, Canada.

[c] Department of Internal Medicine, University of Michigan, 2600 Plymouth Rd.; NCRC B20E Ann Arbor, MI 48109, USA

[d] Department of Human Genetics, Leiden University Medical Center, P.O. Box 9600, 2300RC Leiden, The Netherlands

[e] Integrated Program in Neuroscience, Department of Medicine, McGill University, Room 302 Irving Ludmer Building, 1033 Pine Ave. W. Montreal, Quebec, H3A 1A1, Canada.

[f] Division of Endocrinology, Department of Medicine, McGill University, 1001 boulevard de Decarie, Montreal, Quebec H4A 3J1, Canada.

Keywords:

DVC, area postrema, nucleus of the solitary tract, cell atlas, PDGFRA

Abstract

The dorsal vagal complex (DVC) is a region in the brainstem comprised of an intricate network of specialized cells responsible for sensing and propagating many appetite-related cues. Understanding the dynamics controlling appetite requires deeply exploring the cell types and transitory states harbored in this brain site. We generated a multi-species DVC cell atlas using single nuclei RNAseq (sn-RNAseq), by curating and harmonizing mouse and rat data, which includes >180,000 cells and 123 cell identities at 5 granularities of cellular resolution. We report unique DVC features such as *Kcnj3* expression in Ca^{+}-permeable astrocytes as well as new cell populations like neurons co-expressing *Th* and *Cck*, and a leptin receptor-expressing neuron population in the rat area postrema which is marked by expression of the progenitor marker, *Pdgfra*. In summary, our findings demonstrate a high degree of complexity within the DVC and provide a valuable tool for the study of this metabolic center.

34 Abbreviations

3v	third ventricle
adj.	adjusted
AMPAr	alpha-amino-3-hydroxy-5-methyl-4-isoxazolepropionic acid receptor
AP	area postrema
APNTS	Area postrema and nucleus of the solitary tract
ARH	arcuate nucleus of the hypothalamus
BAM	binary alignment map
CC	central canal
COE	collier/Olf1/EBF transcription factor
diH_2O	distilled water
DMV	dorsal motor nucleus of the vagus
DVC	dorsal vagal complex
FACS	fluorescence-activated cell sorting
FC	fold-change
GABA	gamma-aminobutyric acid
GDF15	growth differentiation factor 15
GIRK1	G protein-coupled inwardly rectifying potassium channel 1
GLP1R	glucagon-like peptide 1 receptor
GFRAL	GDNF family receptor alpha-like
IR	immunoreactivity
LH	lateral hypothalamus
Lnc	long non-coding
ME	median eminence
Neur	neuronal
NG	*Ng2* glial cell
NS	non-significant
NTS	nucleus of the solitary tract

OL	oligodendrocyte
OPC	oligodendrocyte precursor cell
PC	principal component
PDGFRA	Platelet-derived growth factor receptor A
Res.	resolution
RNA-seq	RNA sequencing
smc	smooth muscle cells
snRNA-seq	single-nuclei RNA sequencing
UMAP	uniform manifold approximation and projection
UMI	unique molecular identifiers
v	version
VGLUT2	vesicular glutamate transporter-2
vr	versus

36 1. Introduction

37 Regulating appetite in response to changing environmental conditions to maintain energy balance
38 requires the intricate interplay of multiple organs. Across the central nervous system, multiple
39 discrete brain regions and cell types control appetite[1]. Within the brainstem, the dorsal vagal
40 complex (DVC), comprising the area postrema (AP), nucleus of the solitary tract (NTS) and dorsal
41 motor nucleus of the vagus (DMV), acts as a key nexus point for metabolic signals, evidenced by
42 the dense expression of many relevant hormone receptors[2]. Separately, the DVC also serves
43 as the primary site of gut-based signals via vagal afferents[3-5]. Functionally, the DVC was long
44 considered a site promoting meal termination[6] but growing evidence suggests it also controls
45 long-term energy balance[7].
46
47 Much of the interest in DVC neurons' role in appetite and energy balance stems from their role as
48 therapeutic targets for obesity and anorexia in cancer cachexia[8, 9]. For many years, most
49 pharmacotherapies failed to produce efficacious and long-lasting weight loss in obesity and
50 increase appetite in cancer cachexia[10-12]. More recently, however, the glucagon-like peptide
51 1 receptor (GLP1R) agonists are eclipsing the weight loss achieved by previous generations of
52 therapeutics[13]. While expressed across the central nervous system, GLP1R expression is
53 particularly enriched in DVC neurons[14] and it is the DVC that mediates many of the effects of
54 GLP1R agonists[11]. Separately, an emerging strategy for treating cancer cachexia is inhibiting
55 growth differentiation factor 15 (GDF15) signaling in the DVC by blocking the action of GDNF
56 Family Receptor Alpha Like (GFRAL)[15], the receptor for GDF15[16]. Given the clinical
57 significance of the DVC for this spectrum of conditions, understanding the molecular
58 heterogeneity and function of this region is essential.
59
60 Traditionally, identification and ensuing study of DVC cell types was limited to known
61 neurotransmitter and receptor-expressing cell types. For instance, the cholecystokinin and
62 monoamine-expressing cells, demarcated by tyrosine hydroxylase (*Th*) expression, were
63 previously shown to be non-overlapping cell populations with unique roles in appetite
64 suppression[17]. More recently, the advent of single-cell mRNA sequencing approaches made
65 unbiased molecular censuses of heterogenous populations possible. Such studies focusing on
66 the mouse have revealed the complexity of the mouse DVC, comprised of dozens of

67 transcriptionally distinct cell types[2, 18, 19]. Moving forward, unifying information from multiple
68 single-nuclei RNA sequencing (snRNA-seq) datasets of the DVC into a reference atlas is needed
69 to more fully understand the cells within the DVC and generate a common and scalable
70 classification for cell identities. Such a reference atlas is also needed to contrast the cell types
71 found within the mouse to other research models, including the rat, which are prominent models
72 for DVC biology[2, 20].
73
74 To address this, we generated a comprehensive snRNA-seq based atlas of the mouse and rat
75 DVC. This atlas features mouse and rat labelled cells with increasing granularity and an
76 accompanying computational toolbox including the mouse and rodent atlas label transfer
77 environment using treeArches. The mouse DVC atlas reveals a higher degree of cellular
78 complexity than previously appreciated. The cellular census of the rat DVC exhibits many
79 similarities to the mouse but also rat-specific cells including a novel population of leptin receptor
80 and *Pdgfra*-expressing neurons localized to the AP. Using this unified atlas, we also uncover the
81 cell types that transcriptionally respond to meal consumption which may hold the potential of
82 suppressing appetite without gastrointestinal side effects.
83

84 ## 2. Materials and methods

85 ### 2.1. Experimental design

86 To generate a snRNA-Seq based atlas of the mouse dorsal vagal complex (DVC), we isolated the
87 DVC from 30 adult C57BL/6J mice and subjected them to 10x Genomics-based single-nuclei
88 RNA barcoding and sequencing. Mice were either fasted overnight (n=5), fasted overnight and
89 then refed 2 hours prior to euthanasia (n=10), fed ad libitum (n=5), injected with LiCl (n=5) or
90 injected with vehicle (n=5). Conserved cell clusters across these groups were then identified.
91

92 ### 2.2. Animals

93 All animals were bred in the Unit for Laboratory Animal Medicine at the University of Michigan and
94 the Research Institute of the McGill University Health Centre. Procedures performed were
95 approved by the University of Michigan Committee on the Use and Care of Animals, in
96 accordance with Association for the Assessment and Approval of Laboratory Animal Care and

97 National Institutes of Health guidelines. Alternatively, procedures were approved by the animal
98 care committee of McGill University.
99
100 **2.2.1. Mouse tissue for sn-RNA sequencing assay**
101 Wild-type C57BL/6J mice (Jackson laboratories) were given ad libitum access to food (Purina Lab
102 Diet 5001) and water in temperature-controlled (22°C) rooms on a 12-hour light-dark cycle with
103 daily health checks. Mice were euthanized by isoflurane anesthesia and decapitated, then the
104 brain was removed from the skull and aligned in a brain matrix. The cerebellar cortex was removed
105 and the DVC was micro-dissected and flash frozen in liquid nitrogen (**Fig.S1**). To limit any
106 circadian-driven gene expression changes, all animals were euthanized 4 hours following the
107 onset of the light phase. Frozen tissue was stored at -80°C until use.
108
109 For assessment of feeding-related gene expression, mice were either ad libitum fed or food was
110 removed at the onset of the dark cycle and the animals were fasted overnight. Animals were then
111 euthanized the next morning under ad libitum fed or fasting conditions. A subset of fasted animals
112 (n=5) were provided food and allowed to refeed for 2 hours prior to euthanasia.
113
114 **2.2.2. Mouse and rat tissue collection for *in-situ* hybridization and immunofluorescent**
115 **assays**
116 Animals were provided with ad libitum access to food (Purina Lab Diet 5001) and water in
117 temperature-controlled (22°C) rooms on a 12 h light-dark cycle with daily health status checks.
118 C57BL/6J mice (Jackson laboratories) or Sprague Dawley rats (Jackson laboratoties) were
119 euthanized by isoflurane anesthesia followed by CO_2 asphyxiation. Animals were then trans-
120 cardially perfused with phosphate buffered saline for 3 minutes followed by 5 minutes perfusion
121 with 10% formalin. Brain tissue was then collected and postfixed for 24 hours in 10% formalin
122 before transfer into 30% sucrose for a minimum of 24 hours. Brains were then sectioned as 30
123 μm thick, free-floating sections.
124
125 **2.2.3. Rat tissue collection for snRNA sequencing assays**
126 Wild-type Sprague Dawley rats (Charles River) were provided with ad libitum access to food
127 (Purina Lab Diet 5001) and water in temperature-controlled (22°C) rooms on a 12-hour light-dark

128 cycle with daily health checks. Rats were euthanized by intraperitoneal injections of pentobarbital
129 and decapitated, then the brain was removed from the skull and aligned in a brain matrix. The
130 cerebellar cortex was removed and the DVC was dissected and flash frozen in liquid nitrogen.
131 Frozen tissue was stored at -80°C until use.
132
133 ### 2.3 Isolation of nuclei from DVC tissue
134 Frozen tissue was pooled (5 pooled DVC from mice and 2 DVCs from rats) and homogenized in
135 Lysis Buffer (EZ Prep Nuclei Kit, Sigma-Aldrich) with Protector RNAase Inhibitor (Sigma-Aldrich)
136 and filtered through a 30mm MACS strainer (Miltenyi). Filtered samples were centrifuged at 500
137 rcf for 5 minutes at 4°C, and pelleted nuclei were resuspended in fresh-made wash buffer (10 mM
138 Tris Buffer, pH 8.0, 5 mM KCl, 12.5 mM MgCl2, 1% BSA with RNAse inhibitor) before undergoing
139 a second filtration and centrifugation. The pelleted nuclei were resuspended in wash buffer with
140 propidium iodide (Sigma-Aldrich) and underwent fluorescence-activated cell sorting (FACS) on a
141 MoFlo Astrios Cell Sorter to remove debris. PI+ nuclei were collected and centrifuged at 100 rcf
142 for 5 minutes at 4°C and resuspended in wash buffer to obtain a concentration of 750-1,200
143 nuclei/μL in preparation for sequencing.
144
145 ### 2.4. Single-nuclei RNA-sequencing
146 Library preparation was performed by the Advanced Genomics Core at the University of Michigan.
147 RT mix was added to target approximately 10,000 nuclei recovered per sample and loaded onto
148 the 10× Chromium Controller chip. The Chromium Single Cell 3′ Library and Gel Bead Kit v3,
149 Chromium Chip B Single Cell kit, and Chromium i7 Multiplex Kit were used for subsequent RT,
150 cDNA amplification, and library preparation, as instructed by the manufacturer. Libraries were
151 sequenced on an Illumina NovaSeq 6000 (pair ended with read lengths of 150 nt).
152
153 ### 2.5. Processing of the snRNA-sequencing files
154 From the snRNA-seq, we obtained four FASTQ files (two per sequencing lane, containing forward
155 and reverse sequences respectively) per mouse treatment and two files with the forward and
156 reverse sequences for the rat samples. We pre-processed the murine FASTQ files using either
157 CellRanger 5.0.1 with inclusion of introns or CellRanger 7.0.1 with default parameters (which
158 include intronic sequences) to align sequencing reads to the murine genome[21]. We aligned to

159 the *Mus musculus* refdata-gex-mm10-2020-A reference genome. For the rat files, we used
160 CellRanger 3.0.1 with no introns inclusion and aligned using the *Rattus norvegicus* genome
161 assembly Rnor_6.0[21]. We obtained 110,167 and 13,360 cells from the murine and rat
162 experiments, respectively. In addition to these two datasets, we also used the following steps to
163 process the murine Dowsett dataset[18] publicly available as a raw gene expression matrix set of
164 files. We processed the gene expression matrices in R[22] with Seurat v5 and SeuratObject v5
165 to remove low quality cells[23]. For processing and analysis, R v4.3.1[22] was used. We filtered
166 cells with ≥500 number of genes mapped and >1.22 RNA unique molecular identifiers (UMIs)
167 counts/genes mapped ratio (based on the first 2 percentiles per sample) (**Table S1**).
168 Subsequently, we merged the data per treatment, calculated the median RNA content of clusters
169 at resolution 1.0 and those below the first quartile of the median distribution were removed (**Table**
170 **S2**). Additionally, we used DoubletFinder v2.0.3 based on the expected doublets rates by 10X
171 Genomics after adjusting for homotypic doublets modeled as the sum of squared annotation
172 frequencies[24] (**Table S3**). On each iteration we processed the data with libraries scaled to
173 10,000 UMIs per cell and log-normalized. We identified the most variable genes computing a bin
174 Z-score for dispersion based on 20 bins average expression. We regressed UMI counts and used
175 principal component (PC) analysis for dimensionality reduction on to the top 2,000 most variable
176 genes. We used the first 30 PCs for *k*-nearest neighbors clustering and for uniform manifold
177 approximation and projection (UMAP) projections using Seurat v5[23] default parameters. Murine
178 samples integration in a single matrix was done with Harmony[25], after which clustering and
179 UMAP projections were performed using the harmony embeddings instead of PCs.
180

181 ### 2.6. Mapping of our murine data to existing brain databases

182 We mapped the resulting murine integrated high quality singlets to the celldex v1.12.0 built-in
183 mouse RNA sequencing reference and other four mouse databases[26-29] (**Table S4**) using
184 SingleR v2.4.1[30] and scRNA-seq v2.16.0[31] packages in R[22]. Since each database has its
185 own cell type nomenclature, in our murine dataset we established a 'likely-cell type' to be
186 unanimous among all databases, for example if all databases labeled a cell as 'neuron'. We initially
187 labeled the cells with conflicting or unassigned label by one or more databases as 'unknown'. To
188 confirm the cell type of all the cells labeled and to identify the unknown cell identities, we mapped
189 473 markers from the literature. For this, the average expression per marker gene was obtained

190 on scaled data for each cluster at resolution 1.0 (i.e. 48 clusters) (Table S5). We also manually
191 visualized UMAP projections from all these markers in our dataset. Some clusters (e.g. cluster
192 27) showed in the previous step to contain cells belonging to different cell types, so we subset
193 and reprocessed these clusters using the Harmony embeddings to assign their cell identity based
194 on marker expression at the lowest resolution level that allowed to separate them.
195

196 ### 2.7. Assigning high resolution clustering-based cell identity in the murine dataset

197 In the murine dataset, for all non-neuronal clusters at resolution 1.0 gene expression markers
198 were obtained using the FindConservedMarkers function from Seurat v5[23] package in R[22].
199 The function was run using the MAST algorithm[32] on scaled data with a log fold-change (FC)
200 threshold of 0.25. Only upregulated marker genes detected on 40% of all cells in that cluster,
201 were retained. Since the FindConservedMarkers gives a log2FC output per sample, we calculated
202 the average log2FC across samples and the proportion of samples for which a gene had an
203 adjusted p-value ≤0.05. A marker gene was considered as such if it had an average log2FC>1
204 across samples and was significant (i.e. had an adjusted p-value ≤0.05) in more than 80% of the
205 samples. Furthermore, neurons were subset, reprocessed and subjected to new clustering
206 through Seurat v5[23]. We obtained the gene markers per cluster at resolution 1.0 as described.
207 We named the clusters based on the known functions of the upregulated/downregulated genes
208 (e.g. myelinating oligodendrocytes), peculiarities of the cell groups (e.g. Ca^{+}-permeable
209 astrocytes) or their upregulated gene expression markers if the previous methods were unsuitable
210 (e.g. Ano2 neurons) (Table S6). All visualizations, unless otherwise stated, were done using
211 ggplot2 v3.5.0 and ComplexHeatmap v2.18.0 packages in R[22].
212

213 ### 2.8. Oligodendrocytes trajectory inference

214 We subset the oligodendrocytes (i.e. pre-myelinating, myelinating intermediate and myelinating)
215 in our murine dataset and placed each cell on an inferred cellular trajectory using their
216 transcriptomic data in R[22]. We used the SCORPIUS v1.0.9 package[33] with default
217 parameters to perform dimensionality reduction by PCA on log-normalized counts and to obtain
218 the trajectory image, with a random seed of 1,000. We additionally performed the analysis on the
219 Harmony embeddings from the original data integration.
220

221 2.9. Gene expression files format interconversions

222 To convert Seurat ('RDS') DVC datasets to 'h5ad' format and vice versa, we used reticulate
223 v1.35.0[34] and anndata 0.7.5.6[35] packages in R[22] with import of scipy, scanpy, numpy and
224 anndata modules from Python v3.9[36]. To convert .txt, .csv and .tsv datasets (i.e. the Ludwig
225 dataset[2], the spinal cord dataset[37] and the cortex/hippocampus database[38]), we converted
226 those to 'h5ad' format in Python v3.9[36].

227

228 2.10. Murine DVC hierarchy construction

229 We converted our murine labeled count matrix to h5ad. We used treeArches[39] in Python
230 v3.9[36] to create a manual tree using the three layers of cellular granularity in our database. We
231 reprocessed the samples using the treeArches pipeline[39] to normalize the count data (counts
232 normalized per cell and then log-normalized). After multiple tests, we determined that the 2,500
233 most variable genes was the optimum parameter for the integration of other datasets based on
234 our murine data, therefore we identified the top 2,500 most variable genes and integrated the
235 samples using scVI and treeArches[39, 40]. This reference latent space obtained after integration
236 was used to generate the UMAP embeddings. This sample integration was done to ensure that
237 inter-sample variations were removed for the cell identity steps. We trained our manual tree based
238 on the cell identity layer-3 labels using default parameters.

239

240 We subset the Ludwig dataset[2] to match the initial 2,500 most variable genes from our datasets
241 and performed surgery to incorporate labels from the Ludwig dataset[2]. The two layers of
242 granularity established by Ludwig[2] were combined in the variable "identity_layer3" to contain
243 the highest granularity of cell identity for neurons and non-neuronal cell types. Next, we
244 normalized the count data as specified for our murine dataset, and mapped the Ludwig dataset
245 on the reference latent space using scArches. We then used the learn_tree function with default
246 parameters for hierarchical progressive learning from scHPL v1.0.5[41] which yielded a hierarchy
247 of harmonized cell labels from both datasets. We printed all trees using matplotlib v3.8.2[42] and
248 scHPL v1.0.5[41]. All steps performed and scripts used in this phase are available in the GitHub
249 repository: https://github.com/LabSabatini/DVC_cell_atlas.

250

251 2.10.1. Corroboration of the validity of our murine cell hierarchy using treeArches
252 prediction modality
253 Using treeArches[39] and its dependencies in Python v3.9[36] we compared the original cell
254 labels in our and Ludwig datasets with the resulting prediction of the label for each cell using our
255 learned hierarchy. We used the predict_labels function from scHPL v1.0.5[41] with default
256 parameters, and the latent representation obtained when we constructed our murine hierarchy.
257 We compared the original and the predicted labels through a heatmap visualization. Next, we
258 predicted the labels of new data, a murine dataset by Dowsett which comprises the NTS, a part
259 of the DVC[18]. We processed the Dowsett data similarly to the Ludwig dataset and obtained the
260 query latent representation. We then used the predict_labels function from scHPL v1.0.5[41] with
261 default parameters to transfer the labels in our hierarchy to the Dowsett dataset based on gene
262 expression similarity among the 2,500 initial most variable genes. We then compared the resulting
263 labels from this prediction to the manual mapping of our cell identities based on maker expression
264 (Table S7) using UMAP embeddings in R[22].
265
266 2.11. Labeling of our rat DVC dataset
267 We processed our rat dataset as previously described to obtain high-quality singlets. Based on
268 the three layers of cell identity that we created to label the murine data from our experiments, we
269 calculated the average expression of the top 5 marker genes for each of the layer-3 identities
270 (except duplicated genes and mouse-specific genes) on every rat cluster to identify those that
271 were equivalent and could be labeled as the murine data (Tables S6 and S8). Since this dataset
272 is smaller than the mouse data, we decided to use clusters at resolution of 2.0 to capture more
273 heterogeneity and delineate better the non-neuronal cell populations. Clusters 27 and 29 were
274 further subset and reclustered since we found them to contain a mix of endothelial cells, mural
275 cells, tanycytes and fibroblasts based on marker expression. Microglia and mixed neurons were
276 sub-clustered as well. The lowest resolution level that allowed to separate populations was used
277 to label the cells. Neurons were also subset and we mapped the murine neuronal classes markers
278 to resolution 2.0 markers which were manually curated to delineate better the different
279 populations within them. For all cell identities, and because we only applied one treatment to the
280 rats (i.e. fed ad libitum), we used the FindMarkers function from Seurat v5[23] package in R[22]

281 to obtain gene expression markers of each rat cell population. The function was run using the
282 MAST algorithm[32] with same parameters used for the murine data (**Table S9**).
283

284 ### 2.12. Construction of the rodent DVC hierarchy

285 We then integrated our rat labeled dataset to the murine samples in Python v3.9[36] using the
286 initial top 2,500 most variable genes initially defined in our mouse data. Incorporation of rat labels
287 was done as previously described for the Ludwig dataset using the learn_tree function for
288 hierarchical progressive learning from scHPL v1.0.5[41]. The cell populations that were not
289 rejected but placed at the bottom of the tree were moved manually to their belonging parent
290 branches. For example, the 'smooth_muscle_rat' label was moved to be a children node of the
291 mural cells node. If the parent branch did not exist, we created it. For example, the
292 'immunity_related_rat' label belonged to a new rat neuronal class, therefore, we incorporated this
293 parent node within the neurons node and then we moved the 'immunity_related_rat' label to be a
294 children node. After manual curation, we re-trained the tree. We printed all trees using matplotlib
295 v3.8.2[42] and scHPL v1.0.5[41]. All steps performed and scripts used in this phase are available
296 at the GitHub repository https://github.com/LabSabatini/DVC_cell_atlas for reproducibility.
297

298 ### 2.13. Mapping gene expression in other brain-site snRNA-seq datasets

299 We downloaded labeled datasets from six brain regions different from the DVC: the HypoMap,
300 spinal cord, cortex, hippocampus, pons and forebrain databases[37, 38, 43, 44]. For the
301 HypoMap data, we subset the database by randomly selecting cells belonging to 32 included
302 hypothalamic samples. We processed the datasets in Seurat v5[23] as previously described and
303 obtained Harmony[25] embeddings to obtain UMAP projections. The labels used in the
304 visualization are the original curated labels provided on each dataset. Neurons were further
305 subset from the processed datasets and reprocessed as previously described. The other datasets
306 were processed in the same manner after subsetting astrocytes. The pons and forebrain data was
307 downloaded using scRNAseq v2.16.0 packages in R through SingleR v2.4.1[30].
308

309 ### 2.14. Differential gene expression analysis in murine treatments

310 We subset the murine dataset neurons and glial cells at layer 2 granularity of identity and obtained
311 differential gene expression for pair-wise comparison of treatments (i.e. refed versus ad libitum

312 fed, refed versus fasted and LiCl versus vehicle injected mice). We used the FindMarkers function
313 from Seurat v5[23] package in R[22] using the MAST algorithm[32] on log-normalized counts
314 with a minimal log fold-change threshold of 0.1 and default parameters. The number of cells per
315 treatment can be found in Table S10.
316

317 ### 2.15. Immunofluorescent staining

318 Free-floating brain sections from mouse and rat were washed with PBS, three times for five
319 minutes. The sections were then blocked for one hour in PBS containing 0.1% Triton X-100 and
320 3% normal donkey serum (Fisher Scientific). The sections were incubated overnight at room
321 temperature with Goat anti-PDGFRA (Invitrogen, CAT#, 1:200), HuC/HuD (Invitrogen, A-21271,
322 1:30). The following day, sections were washed and incubated for two hours with Alexflour488
323 and Cy3 conjugated secondary antibody (Jackson immunoresearch, 1:500). Tissues were then
324 washed three times in PBS before being mounted onto glass slides, covered in mounting media
325 (Fluoromount-G, Southern Biotechnology) and coverslipped. Imaging was performed using an
326 Olympus BX61 microscope and a Zeiss LSM780-NLO laser scanning confocal microscope
327 equipped with IR-OPO lasers at the Molecular Imaging Platform, Research Institute of the McGill
328 University Health Centre (RI-MUHC), Montreal, CA.
329

330 ### 2.16. *In-situ* hybridization and imaging

331 Brain sections containing the DVC from four wild-type C57BL/6J mice obtained as described
332 above, were fixed on glass slides and stored at -20°C for no more than 36 hours. We followed the
333 manufacturer's ACD 323100 user manual for the RNAscope® Multiplex Fluorescent Reagent Kit
334 v2 Assay for fixed frozen tissue samples. Briefly, we rinsed the slides with 1X PBS and incubated
335 them at room temperature for 10 minutes after adding ~1-2 drops of H_2O_2 per section. We
336 removed the H_2O_2 from slides and rinsed them twice with distilled water (diH_2O). Next, we
337 submerged the slides in 200 mL of hot diH_2O for 10 seconds followed by 200mL of RNAscope®
338 1X Target Retrieval Reagent for 5 minutes, using a steamer with lid. After briefly transferring the
339 slides to room temperature diH_2O, we submerged them in 100% ethanol for 3 minutes and
340 allowed them to air dry. We applied approximately 1-2 drops of RNAscope® Protease III to each
341 section and incubated them at 40°C for 30 minutes in a HybEZ™ oven with diH_2O wet paper in
342 the tray. After rinsing the slides with diH_2O, we hybridized the probes at 40°C for 2 hours.

343

344 From this point on, we performed all steps by incubating the slides at 40°C in the HybEZ™ oven
345 with humid tray followed by rinse using RNAscope® 1X Wash Buffer. We applied approximately
346 1-2 drops of RNAscope® reagents AMP1, AMP2, AMP3 and then intercalated HRP channel (15
347 minutes), fluorophore (30 minutes) and HRP blocker (15 minutes) for each channel present in the
348 probe mix. The mix of probes used for the *Th*/*Cck* co-expression assay was RNAscope® Mm-Th-
349 C2 (317621-C2) and Mm-Cck-C3 (402271-C3) diluted in probe diluent as specified in the user
350 manual. For *Hcrt* we used RNAscope® Mm-Hcrt-C2 (490461-C2) and for *Agrp*, Mm-Agrp
351 (400711), in a dilution as specified in the user manual. The used fluorophores were Cy3 for *Cck*
352 and *Hcrt* (1:1,500), and Cy5 for *Th* and *Agrp* (1:1,000) diluted in RNAscope® TSA buffer. DAPI
353 dye (1:1,000) was applied at the end of the assay, and the samples were stored for ~48 hours at
354 -4°C, protected from light, before imaging. We imaged the sections using a Zeiss LSM780-NLO
355 laser scanning confocal microscope with IR-OPO lasers at the Molecular Imaging Platform at the
356 RI-MUHC, Montreal, CA.

357

358 ## 3. Results

359 ### 3.1. The murine dorsal vagal complex cell classes

360 To generate a *de novo* snRNA-seq atlas of the mouse DVC, we isolated the DVC from 30 adult
361 C57BL/6J mice and subjected them to 10X Genomics-based snRNA barcoding and sequencing
362 (**Fig.1A**). From the CellRanger pre-processing pipeline[21] we obtained 110,167 cells of which
363 99,740 were retained after processing. Cell identities were initially mapped to 5 databases from
364 different brain regions and then curated manually using 473 cell identity markers (**Tables S4-S5**).
365 We distinguished clusters of neurons and glial, vascular and connective tissue cells, a first layer
366 of cell identity (**Fig.1B**; **Table S9**). We further describe a second layer of cellular resolution, which
367 are subgroups of the first layer that contain the cell classes (**Fig.1C**; **Table S7**).

368

369 Among the ten neuronal cell classes identified at layer 2 resolution, we found two major groups
370 which we called 'magnaclass1' and 'magnaclass2' (**Fig.S2**). Magnaclass1 neurons predominately
371 express genes required for inhibitory neurotransmission (e.g. *Gad1*, *Gad2*) and share
372 transcriptomic markers with the Sall3-class of neurons, whereas magnaclass2 neurons express
373 mostly excitatory transcripts (e.g. the glutamate transporter VGLUT2) also found in the Lhx2-

374 class and monoamine-class (**Fig.1D-E**; **Fig.S2**). However, as described in other brain areas[45,
375 46], evidence of co-transmission/co-release of multiple primary neurotransmitters was found in at
376 least 55% of neurons regardless of their cell class (**Fig.1D-E**; **Table S11**). We also identified 8
377 transcriptionally distinct neural classes in addition to the magnaclasses. Among these 8 classes
378 we found two neural classes expressing traditionally non-neuronal genes; the Golli and pH-related
379 classes. The Golli-class neurons are a relatively small cluster, comprising ~1% of all neurons.
380 Interestingly, Golli-class neurons express multiple myelin-associated genes such as *Mag* and
381 *Mog*[47-49] normally expressed by oligodendrocytes (**Fig.1D**; **Table S6**). Additionally, we
382 identified a class of neurons with genes normally upregulated in astrocytes (e.g. *Slc6a11*) and
383 related to clearance and uptake of glutamate, gamma-aminobutyric acid (GABA), Ca^{+} and
384 bicarbonate [50, 51], which we named 'pH-related class' (**Table S6**). Similar to Golli-class
385 neurons, pH-related neurons were a relatively rare cluster (<1% of all neurons). While the
386 corelautus-class neurons express very few genes at higher levels, among them are *Cdk8*, *Lars2*,
387 *Gabra6* and *Fat2*. Expression of *Cdk8* is largely absent from the DVC but is enriched within the
388 DVC-adjacent hypoglossal nucleus (**Fig.S3**) suggesting these cells are hypoglossal neurons. We
389 also identified the Lhx2-Class which was enriched for the Parvalbumin (*Pvalb*) gene whose
390 expression is largely excluded from the DVC. As *Pvalb* is highly expressed in the neighbouring
391 cuneate nucleus (**Fig.S3**), we posit this class may belong to this anatomically adjacent area which
392 was captured in our dissection. When interrogating snRNA-seq data from the hypothalamus[43]
393 (**Fig.S4**), another brain site important for energy balance, we could not find clusters sharing all
394 markers with our neuronal classes, indicating DVC-specific neuronal programs (**Fig.S4C**).
395

396 **3.2. The murine DVC cells at their highest resolution**

397 To better define the heterogeneity of the mouse DVC, we further assigned a clustering-based
398 third layer of cellular resolution resulting in fifty cell identities, of which 15 are non-neuronal
399 (**Fig.2A**). At this resolution we differentiated between two major groups of astrocytes. Differential
400 expression in synapse-related factors revealed a group of astrocytes with high expression of the
401 inwardly rectifying GIRK1 (*Kcnj3*) channel[52] and lack of expression of the AMPAr subunit GluA2
402 (*Gria2*), additionally rendering them K^{+}/Na^{+}/Ca^{+}-permeable[53, 54] (**Fig.2B**). We speculate these
403 astrocytes are specific to the DVC as we could not find *Kcnj3*+; *Gria2*- astrocytes in the
404 hypothalamus, forebrain, cortex or hippocampus[38, 43, 44] (**Fig.S4D**; **Fig.S5**). Furthermore,

405 although some regions close to the DVC such as pons and the spinal cord show some co-
406 expression of *Kcnj3* and *Gfap*, the patterns are not to the same extent as observed in the DVC
407 [44] (**Fig.S5F-G**). In addition, we distinguished a spectrum of DVC mature oligodendrocytes,
408 including a group resembling the intermediate oligodendrocytes described in the other brain sites
409 that decrease in number with age[37, 55] (**Fig.2C**). This gradient of expression of markers
410 including *Fyn*, *Opalin* and *Anln* in oligodendrocytes (**Fig.2C**), do not respond to a developmental
411 trajectory (**Fig.S6**). Although 'myelinating-intermediate' and 'myelinating' oligodendrocytes
412 include cells with overlapping gene expression programs, there is no evidence that each
413 oligodendrocyte will follow a single trajectory (**Fig.S6**). Furthermore, to properly separate some
414 cell identities, we performed sub-clustering in three DVC clusters (i.e. clusters 23, 26 and 27)
415 (**Fig.S7A**). This permitted us to label pre-myelinating oligodendrocytes, endothelial and mural
416 cells, and distinguish two fibroblast sub-types (**Fig.S7**). One of these subtypes expresses high
417 *Stk39* previously described in fibroblast stress-response[56] and so was termed 's-fibroblasts' for
418 stress-associated fibroblasts (**Fig.S7B**), which we failed to detect in the hypothalamus (**Fig.S4E**).
419 Additionally, we excluded the possibility of monocytes in our microglial data (**Fig.S8A**), which had
420 no evidence of microglial activation as we mapped minimal levels of the activation genes *Cxcl10*,
421 *Cd5*, *Cxcl9* and *Zbp1*[57], therefore we posit that our DVC microglial cells are in a basal state
422 (**Fig.S8B**). To further evaluate possible activation states in microglia, we performed sub-clustering
423 and evaluated their marker genes (**Fig.S8C**). We have identified a group of microglia expressing
424 oligodendrocyte markers and resembling a subpopulation of hippocampal microglia in an
425 Alzheimer's disease model which is disease-protective and synaptic-function-supporting[58], and
426 a cortical/subcortical phagocytic subpopulation in a multiple sclerosis model[59]. A second group
427 expresses *Ndrg2* and receptors for GABA and glutamate which have been related to microglia
428 that may induce neuronal damage[60, 61] (**Fig.S8D**).
429
430 We also obtained the DVC gene expression markers of the main cell types in the central nervous
431 system and neurons (**Fig.2D**). To more thoroughly classify DVC neural types, we subset and re-
432 clustered the 10 neural classes from layer 2 which resulted in 35 neuronal identities as a third
433 layer of granularity (**Fig.3A**; **Table S6**). These identities include 'preganglionic' or *Chat*-expressing
434 neurons and a large number of neurons with unspecific markers which we called 'mixed neurons'
435 (**Table S6**). Of the mixed neuron classes, two are largely excitatory (Mixed neurons 3 and 4) and

436 two largely inhibitory, however, cells in the four mixed neuron classes share similar transcriptional
437 profiles with many other neural classes. When we performed sub-clustering on mixed neurons,
438 we could distinguish a total of 10 subtypes from the original 4 mixed neuronal identities (**Fig.S9**);
439 however, transcriptional differences between these were subtle. Interestingly, a mixed neurons-
440 like group of cells was previously described in the murine hypothalamus[26], suggesting multiple
441 brain sites may contain neurons which lack highly differentiable transcriptional programs from
442 snRNA-sequencing data.
443
444 Additionally, we split the monoamine-class into four layer-3 cell identities (i.e. M0, M1, M2 and
445 M3) with specific cell markers (**Fig.3B**; **Table S6**). M0 and M1 neurons express genes for enzymes
446 synthesizing norepinephrine and serotonin, but M0 expresses minimal levels of the transporter
447 VMAT2 (*Slc18a2*) (**Fig.3C**; **Table S6**). Due to the low proportion of cells expressing *Th* and *Tph2*
448 in M2 and M3 neurons, we consider them monoamine-modulators as they seem to synthesize
449 trace amines (**Fig.3C**; **Table S6**). Of note, the receptor for GDF15, GFRAL, is expressed heavily
450 by a subset of M0 neurons, some of which co-express the calcium sensing receptor (*Casr*) gene
451 (**Fig.3C**).
452
453 We named 'GLP1' a neuronal cluster with high expression of the pre-proglucagon gene (*Gcg*)
454 (**Fig.3D**; **Table S6**), which also expresses high levels of both the prolactin and leptin receptors[62]
455 (**Fig.3E**). Additionally, these cells have the highest proportion of DVC neuronal co-expression of
456 glutamate- and GABA-related genes (**Fig.3F**); mainly *Gad2* with considerably lower expression of
457 *Slc32a1*.
458
459 In our analysis we found a subset of monoaminergic neurons that express the cholecystokinin
460 (*Cck*) gene (**Fig.4A**). While the *Cck* and *Th*-expressing DVC neurons are considered to be non-
461 overlapping cell types with distinct physiologies[17, 63], but we quantified >10% of the *Th*-
462 expressing neurons also expressing *Cck* in our snRNA-seq data. We further confirmed co-
463 expression of *Th* and *Cck* results by *in-situ* hybridization (**Fig.4B**). The majority of this overlap
464 occurs in cells belonging to the COE-Atp10a and monoamine class (i.e. M0, M3) cell identities
465 (**Fig.4A**).
466

467 3.3. The murine DVC cell atlas

468 To generate a comprehensive murine DVC database from multiple datasets, we utilized
469 treeArches[39] to harmonize our snRNA-seq DVC labels with that from a publication by Ludwig
470 and collaborators (i.e. the 'Ludwig dataset')[2] (Fig.5A-B). After building our initial cell hierarchy
471 (Fig.S10), we integrated our dataset with the Ludwig dataset, giving a total of 171,868 cells
472 (Fig.5B). Next, the labeled cell identities from the Ludwig dataset[2] were incorporated into our
473 tree based on the similarity between the transcriptomic programs of our labeled identities and the
474 Ludwig-labeled identities using progressive learning through scHPL[41] (Fig.5A). Some of the
475 Ludwig dataset identities failed to be incorporated into our tree, like the oligodendrocyte precursor
476 cells (OPCs), which contain a mix of OPCs and pre-myelinating oligodendrocytes (Fig.S11A). The
477 mix of cell programs makes it impossible for treeArches to correctly add one branch of the Ludwig
478 OPCs to the tree as ideally it would be added as a subpopulation of both the OPCs and pre-
479 myelinating oligodendrocytes, which is not biologically possible. The resultant murine hierarchy
480 has a fourth layer of cellular resolution as some of Ludwig identities, mainly neurons, are
481 subgroups of our cell identities (Fig.S11B).
482
483 We confirmed the validity of our cell hierarchy using three methods. First, by using the learned
484 model to predict the labels of the cells we used to develop them (i.e. this study and the Ludwig
485 dataset), for which we obtained highly concordant cell labeling (Fig.5C). Secondly, we used the
486 learned model to predict the labels of another publicly available dataset from Dowsett and
487 collaborators (i.e. the 'Dowsett dataset')[18] (Fig.5D). Using this approach, we were able to
488 successfully label 95% of these cells at high resolution (i.e. layer 3 or 4 of cell identity granularity);
489 further validating our combined DVC labels. Finally, we manually mapped the marker genes from
490 Ludwig[2] and Dowsett[18] neuronal clusters in our dataset and confirmed the sub-groups of
491 neurons among our identities pointed out by treeArches (Fig.S11B).
492

493 3.4. An integrated rodent DVC cell hierarchy

494 To identify rat DVC cell clusters and subclusters and contrast these with the mouse DVC atlas,
495 we generated a *de novo* ad libitum-fed rat dataset (cells n=12,167) (Fig.6A) and labeled it by
496 mapping the top 5 gene expression markers of each of our murine layer-3 cell identities (Table
497 S8). After manual curation at three granularities (Fig.6B-C; Table S9), we obtained 52 DVC rat

498 identities at high cellular resolution (**Fig.6C**) including a small group of 'unspecific' cells (n=35)
499 that we could not confidently label because its top gene expression markers have unknown
500 functions and none of our known identities' genes clearly marked this population (**Fig.6B-C**; **Table**
501 **S8**).
502
503 We established 10, layer-3 neuronal identities not previously found in the murine data (**Fig.6C**;
504 **Fig.S12A**; **Table S9**). Notably, two of those did not belong to any of the existing murine neuronal
505 classes (i.e. layer-2 of cellular granularity), therefore we created two new layer-2 classes (**Fig.6B**).
506 One of these, the immunity-related neurons, have high *Csf1r* expression, as well as cystatin C
507 and *Inpp5d* which are commonly associated with immunity-related processes in microglia and
508 with immunomodulation in cancer[64, 65] (**Fig.7**; **Table S10**). The second neural class identified
509 in rat but not mouse DVC were the 'Pdgfra neurons' (**Fig.7**). These neurons express *Pdgfra*,
510 *Arhgap31* and *Itga9*, known markers for progenitor cells for which we named this cell class 'ortus-
511 akin' (Latin: 'origin') because they are similar to cells giving origin to other cells[66] (**Fig.7A**; **Table**
512 **S10**). Interestingly, this neuronal class not only expressed *Pdgfra*, but also other OPC signature
513 genes (**Fig.7A**). Mapping the expression levels of metabolic-associated receptors revealed that a
514 subset (~15%) of both immunity-akin and ortus-akin express detectable *Gfral* mRNA but this is
515 likely an underrepresentation due to the challenges in detecting lowly expressed transcripts such
516 as *Gfral*. Prolactin receptor and leptin receptor (**Fig.7B**) were also found to be expresses by these
517 neurons, although they seem to have a varied neurotransmitter profile (**Fig.S12B**). To confirm the
518 presence of *Pdgfra*-expressing neurons in the rat DVC, we performed immunostaining in the
519 mouse and rat brainstem. Within the mouse, we found PDGFRA-immunoreactivity(IR) in the two
520 morphologically distinct cells; matching OPC and blood vessel-associated fibroblast
521 morphologies(**Fig.7C**). However, within the rat, we identified PDGFRA-IR in cells with three
522 morphologies, one of which resembled neurons with an enlarged cell body and protruding cellular
523 processes (**Fig.7C**). To determine if these PDGFRA-IR cells were neurons, we co-stained with the
524 neural marker, HuC/D and noted several PDGFRA and HuC/D copositive cells (**Fig.7D**);
525 confirming our sequencing data that a PDGFRA-expressing neural class exists in the rat DVC and
526 localizing these cells to the area postrema.
527

528 Other differences found between mouse and rat DVC expression includes increased expression
529 of the leptin receptor in neurons as well as cholecystokinin (**Fig. S13**).
530
531 To construct an integrated rodent DVC cell atlas, we incorporated the labeled rat dataset into our
532 hierarchy using treeArches[39] (**Fig.8**). The rat data was projected onto the mouse datasets
533 (**Fig.8A**) and the 42 high resolution rat cell identities were appended to the tree (**Fig.8B**; **Fig.S13**).
534 The final hierarchy has 123 labels of which 99 are high resolution according to our cellular
535 granularity (i.e. layers 3 to 5) (**Fig.8B**). In addition it has 20 layer-2 identities and 7 cell identities
536 that are novel from the rat dataset (**Fig.8B**).
537
538 ### 3.5. *Hcrt* and *Agrp* expression in the DVC
539 Since *Agrp*-expressing cells have been recently described within the DVC[67], we mapped this
540 and other neuropeptide genes in DVC neurons. Surprisingly, we found *Hcrt* and *Agrp* mRNA in
541 neurons in our dataset (**Fig.S14A**). We then performed *in-situ* hybridizations for these transcripts
542 in both the mouse hypothalamus and DVC. While both *Hcrt* and *Agrp* were readily detectable in
543 the hypothalamus, we failed to observe signal within the DVC (**Fig.S14B**). Since we also found
544 expression of *Hcrt* and *Agrp* in neurons of the Dowsett and Ludwig datasets[2, 18] (**Fig.S14C**),
545 we then mapped the sequenced reads from these transcripts and confirmed that most of them
546 mapped to intronic and non-coding regions of these genes (**Fig.S14D**). Furthermore, our rat DVC
547 dataset was pre-processed excluding introns from the reads mapping, and the *Hcrt* and *Agrp*
548 expression levels observed is minimal (**Fig.S14E**), which is in agreement with the non-coding
549 location of the reads in mouse DVC. These data explain absence of signal from our *in-situ*
550 hybridizations and suggests DVC cells do not produce HCRT or AGRP neuropeptides.
551
552 ### 3.6. Meal-related transcriptional programs in the murine DVC
553 As the DVC acts as a primary node for meal-related signals[68], we wanted to define which of our
554 cell identities responded to meal consumption and thus performed differential gene expression
555 analysis between DVC cell types from mice that were euthanized under fasting conditions, with
556 ad libitum access to food or two hours post-refeeding following an overnight fast (**Fig.1A**; **Fig.9**).
557 This analysis revealed widespread transcriptional changes across nearly every neural cell identity,
558 the exceptions being corelautus, Golli class and pH classes (**Fig.9A**). Additionally, the size of the

559 transcriptional changes were relatively small, with approximately 90% of the differentially
560 expressed genes having increases or decreases between 0.5 and 1.0 log2 fold-change, with only
561 ~10% of the gene changes being ≥1 log2 fold-change between conditions (Fig.9A). Of the
562 responding neurons, magnaclasses 1 and 2, which represent large populations of predominately
563 inhibitory and excitatory neurons (Fig.S2), showed the greatest number of differentially expressed
564 genes following refeeding for both comparisons refed versus fasting, and refed versus ad libitum
565 food access (Fig.9A). To understand how refeeding transcriptionally alters inhibitory compared
566 with excitatory DVC neurons, we compared differentially expressed genes between these two
567 classes across conditions. Intriguingly, despite being in transcriptionally distinct classes, we found
568 meal consumption altered many of the same genes (Fig.9B-D), suggesting these cells may be
569 receiving similar postprandial signals which are propagated via these cells in unique manners.
570 This is supported by the similar receptor expression profile of magnaclass 1 and 2 (Fig.S15). One
571 notable exception is *Cckbr* which is upregulated in magnaclass 2 and downregulated in
572 magnaclass 1 in refeeding when compared with ad libitum fed mice(Table S12). We also note that
573 oligodendrocytes contained the highest number of differentially expressed genes in refeeding
574 (Fig.9A). While the roles of oligodendrocytes in refeeding responses within the DVC have yet to
575 be determined and the biologic significance of these changes are presently unclear, DVC
576 oligodendrocytes also have robust transcriptional responses in response to fasting[18];
577 suggesting these cells are sensitive to both positive and negative energy balance associated-
578 cues and may have important roles in regulating energy homeostasis.
579

580 ## 4. Discussion

581 The recent success of DVC-based therapies[13, 69] has moved DVC biology to the forefront of
582 weight control therapies and there is now clear clinical impetus to fully define DVC cell types and
583 their functions. Previous studies detailing DVC cell types describe a high degree of
584 heterogeneity[2, 18, 19], however, these studies lacked an in-depth analysis of neurotransmitter
585 profiles of neurons, any cross-species evaluation of DVC cell types, or an analysis of how meal
586 consumption transcriptionally regulates these cells. We therefore developed *de novo* mouse and
587 rat DVC cell atlases to address these points.
588

589 To more fully describe the cellular complexity within the DVC, we combined a pipeline of cell label
590 transfer using brain existing published datasets and thorough curation of cell identities, which
591 resulted in a 4-layer mouse cell hierarchy and a 5-layer rodent cell hierarchy of the DVC. Within
592 this hierarchy we found several unique features of DVC glial cells. First, we found Ca^{+}-permeable
593 astrocytes in the DVC in which *Gfap* is almost exclusively expressed and they coexpress *Kcnj3*
594 (GIRK1 potassium channel). These cells largely lack *Gria2*, consistent with findings in Bergmann
595 glial cells in which colocalization of *Gria2* and GFAP was found to alter neuron-glial
596 interactions[70]. The heterogeneity of astrocytes across, and even within, spatially distinct CNS
597 sites is becoming increasingly apparent[71] and our finding of DVC-specific astrocyte
598 transcriptional profiles further supports this. When we compared Ca^{+}-permeable DVC astrocytes
599 to hypothalamic astrocytes[43], we found the same expression pattern with minimal overlap
600 between *Gria2* and *Gfap.* However, DVC astrocytes seem to have some unique properties when
601 compared with hypothalamic, cortical and hippocampal astrocytes. Principally, DVC astrocytes
602 express the GIRK1 channel, likely rendering them less excitable[72]. As astrocytes have well
603 established roles in maintaining the blood brain barrier function[73], and the pattern of GFAP in
604 the DVC is largely restricted to the boundary separating the AP and NTS, it is possible these DVC-
605 specific astrocytes have specialized functions in regulating blood brain barrier permeability.
606
607 Additionally, while we identified hypothalamic fibroblasts which express high *Aldh1a1* similar to
608 the DVC p-fibroblasts, we failed to find a group equivalent to s-fibroblasts. Other cell populations
609 seem to be consistent to what has been found in other brain sites, like the intermediate
610 oligodendrocytes that are found enriched in the hypothalamus and the corpus callosum in
611 mice[55]. In summary, these findings show that while certain DVC glial cells share identities with
612 glial cells from other CNS sites, there are also DVC-specific glial cells.
613
614 Within the mouse neural classes, we found overlap between *Cck* and *Th*-expressing cells. As
615 these cells have previously been described as non-overlapping, this was unexpected[17]. Our *in-*
616 *situ* hybridization confirmed the presence of *Cck*/*Th* positive cells within the NTS and AP. We
617 believe the discrepancy may be due to detection methods as these cells were initially defined as
618 non-overlapping using immunofluorescent detection of TH protein and a *Cck* genetic reporter[17].
619 Functional studies of *Cck*- and *Th*-expressing neurons within the NTS demonstrate these cells

620 have somewhat distinct roles; while both reduce appetite, *Cck* neurons are strongly aversive
621 whereas *Th*-labelled neurons are non-aversive[74]. While no functional characterization of *Cck*
622 and *Th* neurons of the AP has been performed, we posit that as some *Th*-expressing AP neurons
623 also express *Gfral* and *Casr*; both having potently aversive ligands (e.g. GDF15,
624 deoxynivalenol)[16, 75]; they are likely to mediate aversive anorexia. The role of dual *Cck/Th*
625 positive neurons remains to be determined.
626
627 While AGRP expression has long been considered to be hypothalamic-exclusive, a recent report
628 describes *Agrp*-expressing cells within the mouse DVC[67], i n part from the detection of Agrp
629 mRNA in scRNA-Seq data. Similarly, we also detected transcripts for both *Agrp* and *Hcrt* in our
630 snRNA-Seq data but failed to detect any transcripts within the DVC by *in-situ* hybridizations. One
631 possible explanation for the discrepancy between the snRNA-Seq data and our *in-situ*
632 hybridizations data is that the snRNA-Seq mRNA reads for*Agrp* and *Hcrt* gene overwhelmingly
633 mapped to non-coding regions, of the respective genes. Combined, these data suggests to us
634 that neither AGRP or HCRT neuropeptides are produced by DVC cells in rodents.
635
636 We show the presence of neurons with seemingly mixed programs in the DVC, which we called
637 'mixed neurons'. Similar groups have been described in the hypothalamus[26] suggesting that
638 some neurons may have hybrid-functionalities. These mixed neurons share many transcriptomic
639 markers expression with many other cell identities, and may require the use of other technologies
640 to fully identify them anatomically in the brain.
641
642 To perform a cross-species analysis, we generated a rat-based DVC atlas and compared it with
643 the mouse DVC. Our rat dataset was smaller than the mouse data, it is possible some of the of
644 the new neuronal cell identities (e.g. M_sema, M4) may contain cells belonging to multiple cell
645 types, as treeArches did not appended these identities to the tree. Despite this, we corroborated
646 two new cell types in the rat DVC that are not present in mice the *Pdgfa*-expressing (ortus-akin
647 class) and the immunity-related neurons. *Pdgfra* is a well described marker gene for OPCs and
648 fibroblasts within the central nervous system[66] but, to our knowledge, has not been associated
649 with neurons. Notably, although the PDGFRA immuno-signal in HuC/D+ neurons is clearly
650 discernible, it is less intense than in OPCs and fibroblasts, in agreement with expression levels

651 from our snRNA-Seq data. Since it was previously demonstrated that OPCs can give rise to
652 neurons in the adult brain[76] and there is evidence of neurogenesis in the AP following amylin
653 administration in rats[77], it is possible that these PDGFRA+/HuCD+ cells in the AP represent a
654 transient stage of PDGFRA+ OPCs differentiating into neurons.
655
656 Regardless of their maturity, we speculate that the Pdgfra neurons (ortus-akin class) have roles
657 in appetite regulation as they express leptin receptor and *Gfral*. Interestingly, while multiple studies
658 have failed to detect *Lepr* via Cre-based reporters[62, 78] or leptin-induced phosphorylated
659 STAT3 in the AP of mice[79], *Lepr* and leptin-induced phosphorylated STAT3 are detectable
660 within the rat AP[80-82]. We believe one explanation for this species discrepancy in *Lepr*
661 expression is the absence of the ortus class neurons in mice. Future studies are needed to
662 characterize these cells and determine whether their presence is found in other mammals
663 including humans.
664
665 DVC-targeting obesity therapeutics, including amylin and GLP1 mimetics, produce clinically
666 relevant weight loss but are associated with multiple gastrointestinal adverse events and there is
667 a need to develop new obesity therapies that can reduce appetite without unwanted
668 gastrointestinal side effects[83]. Indeed, the DVC cells that control appetite suppression and
669 nausea are separable[11, 74], making targeting such cells an attractive target for
670 pharmacotherapy. As meal consumption is generally not associated with gastrointestinal distress,
671 we sought to identify refeeding responsive cells within the mouse DVC. From this analysis, we
672 found nearly all neural cell identities are transcriptionally altered by meal consumption. We also
673 found the magnitude of transcriptional changes was relatively small, regardless of the cell class
674 examined. While relatively small, the scale of the transcriptional changes in response to refeeding
675 are similar to many of the gene expression changes observed in *Agrp*-neurons following 16 hours
676 food deprivation[43]. Regardless of whether this is a technical limitation of snRNA-Seq methods
677 or accurately reflects the scale of transcriptional changes in the DVC, utilizing transcriptional
678 responses to refeeding to identify neural classes as targets for pharmacotherapy is unlikely to
679 yield specific and targetable pathways.
680

681 In general, one limitation in our study is that it is based on nuclear RNA which may reflect a fraction
682 of biological changes. Using nuclear isolation facilitates generating to have single-neuron data[84]
683 since obtaining viable whole neurons (including all their processes) is very challenging. Previous
684 studies on the relationship between nuclear and cellular RNA content in brain show that nuclear
685 sequencing reads may map to intronic regions of genes in higher proportion[85]. Although this
686 does not appear to impact gene expression analysis for neurons in the current pipelines like the
687 ones we used for our mouse data[85], it is possible that some biological features such as
688 microglial activation state, are not fully recovered using nuclear RNA[86]. Although we performed
689 sub-clustering in the mouse microgia and assessment of the resulting marker genes for each
690 group, we did not find evidence of activation possibly due to this matter. Separately, for meal
691 consumption, we were unable to analyze responses in individual mice as pooling DVCs from
692 individual mice was the most amenable option to maximize nuclei for in our pipeline. As we pooled
693 DVCs from both sexes, this limited our ability to detect sexual dimorphic cell class proportions
694 and gene expression levels.
695

696 ## 5. Conclusion

697 As the amount of snRNA-Seq data performed on the DVC continues to grow, there is a need for
698 a common, scalable label set that can be applied to new studies and integrate new sequencing
699 data. To develop such a label set, we started with a *de novo* DVC atlas, we generated three layers
700 of cellular granularity for both neural and non-neuronal cell types. Then, using the treeArches
701 pipeline[39] we harmonized our snRNA-Seq labels with the Ludwig dataset[2] and increased our
702 cellular granularity from three to four layers of resolution. Manually curating and harmonizing our
703 dataset enhanced the ability of our cell atlas to capture the complexity of the DVC neurons since
704 not all groups seem to contain easily delineable subgroups of cells. For example, eleven of the
705 labels incorporated into our cell hierarchy in this pipeline belong to the monoaminergic neuronal
706 class, which seem to encompass multiple subgroups of specialized cells. We further constructed
707 the rodent DVC cell atlas which resulted in a fifth layer of cell identity to the monoaminergic M3
708 neurons. Although the number of identities increases as layers are more specific, this gives this
709 unified atlas greater adaptability to different research needs. Additionally, our labels can be
710 accurately harmonized with new databases regardless of size and new DVC snRNA-Seq data can

711 be added to the tree to generate new branches. Thus, our unified rodent DVC atlas is highly
712 amenable to future research elucidating new biologic and therapeutic insights into DVC cell types.
713

714 ## 6. Acknowledgements

715 We would like to thank authors of the Ludwig and the Dowsett publications for making publicly
716 available their datasets. We thank M. Myers Jr. for the valuable help provided; S. Hebert and S.
717 Bailey for their insights and suggestions in regards to the bioinformatic analysis; members of the
718 Kokoeva lab for their insights on the *in-situ* hybridization and immunohistochemistry pipelines; S.
719 Feng and M. Fu for technical assistance for images acquisition at the Molecular Imaging Platform
720 at the RI-MUHC, and A. Duensing for assistance with relevant file transfer.
721

722 ## 7. Author contributions

723 Conceptualization: CH and PS
724 Methodology: CH, AB, LM, MK and PS
725 Sample collection: AB and PS
726 Software: CH, LM and HJM
727 Data analysis: CH, LM, MK and PS
728 Data curation: CH and HJM
729 Validation of findings: CH, FS, HJM and PS
730 Imaging: CH and PS
731 Visualization: CH, MK and PS
732 Supervision: CH and PS
733 Writing—original draft: CH and PS —review and editing: CH, AB, LM, FS, HJM, MK and PS
734 Funding acquisition: MK and PS
735

736 ## 8. Funding

737 This research was also supported by grants from Canadian Institutes for Health Research
738 (PJT180590 for PVS and 202010PJT for MK) the Natural Sciences and Engineering Research
739 Council of Canada (RGPIN-2022-03390). HJM was funded in part by the Canada First Research
740 Excellence Fund and Fonds de recherche du Quebec, awarded to the Healthy Brains, Healthy
741 Lives initiative.

742

743 ## 9. Declaration of interests

744 The authors declare that they have no competing interests.

745

746 ## 10. Data statement

747 All data needed to evaluate the conclusions in the paper are present in the paper and/or the
748 Supplementary Materials. FASTQ files have been deposited in the NCBI Sequence Read Archive
749 (Accession: PRJNA1161292). In addition, our murine and rat datasets have been made available
750 for visualization and analysis through the Broad Institute Single Cell Portal
751 (https://singlecell.broadinstitute.org/single_cell/study/SCP2773). The labels from our cell atlas
752 can be transferred to new datasets through treeArches using the available hosted Jupyter
753 Notebook in Google Colab for the mouse data
754 (https://colab.research.google.com/drive/1v983gcQxIwBN-
755 4lGx18JXPweZoKqMbwX#scrollTo=SJTZppZWa-63), and for the rodent data
756 (https://colab.research.google.com/drive/10tAmfRosMscuBak6wHX80TgdEBsHeWQB#scrollTo
757 =941ab5c1-8910-4e67-a632-4d18601d45b4). Original code used for constructing the murine
758 and rodent cell hierarchies and predicting labels using treeArches are available in the GitHub
759 repository https://github.com/LabSabatini/DVC_cell_atlas.

760

761 References

762 [1] L. Gautron, J.K. Elmquist, K.W. Williams, Neural control of energy balance: translating
763 circuits to therapies, Cell. 161 (2015) 133-45. 10.1016/j.cell.2015.02.023.

764 [2] M.Q. Ludwig, W. Cheng, D. Gordian, J. Lee, S.J. Paulsen, S.N. Hansen, et al., A genetic
765 map of the mouse dorsal vagal complex and its role in obesity, Nat Metab. 3 (2021) 530-45.
766 10.1038/s42255-021-00363-1.

767 [3] L. Bai, S. Mesgarzadeh, K.S. Ramesh, E.L. Huey, Y. Liu, L.A. Gray, et al., Genetic
768 Identification of Vagal Sensory Neurons That Control Feeding, Cell. 179 (2019) 1129-43 e23.
769 10.1016/j.cell.2019.10.031.

770 [4] W. Han, L.A. Tellez, M.H. Perkins, I.O. Perez, T. Qu, J. Ferreira, et al., A Neural Circuit for
771 Gut-Induced Reward, Cell. 175 (2018) 665-78 e23. 10.1016/j.cell.2018.08.049.

772 [5] E.K. Williams, R.B. Chang, D.E. Strochlic, B.D. Umans, B.B. Lowell, S.D. Liberles, Sensory
773 Neurons that Detect Stretch and Nutrients in the Digestive System, Cell. 166 (2016) 209-21.
774 10.1016/j.cell.2016.05.011.

775 [6] M.W. Schwartz, Central nervous system regulation of food intake, Obesity (Silver Spring). 14
776 Suppl 1 (2006) 1S-8S. 10.1038/oby.2006.275.

777 [7] W. Cheng, E. Ndoka, J.N. Maung, W. Pan, A.C. Rupp, C.J. Rhodes, et al., NTS Prlh
778 overcomes orexigenic stimuli and ameliorates dietary and genetic forms of obesity, Nat
779 Commun. 12 (2021) 5175. 10.1038/s41467-021-25525-3.

780 [8] S.Z. Yanovski, J.A. Yanovski, Long-term drug treatment for obesity: a systematic and clinical
781 review, JAMA. 311 (2014) 74-86. 10.1001/jama.2013.281361.

782 [9] T. Borner, C.G. Liberini, T.A. Lutz, T. Riediger, Brainstem GLP-1 signalling contributes to
783 cancer anorexia-cachexia syndrome in the rat, Neuropharmacology. 131 (2018) 282-90.
784 10.1016/j.neuropharm.2017.12.024.

785 [10] S.M. Advani, P.G. Advani, H.M. VonVille, S.H. Jafri, Pharmacological management of
786 cachexia in adult cancer patients: a systematic review of clinical trials, BMC Cancer. 18 (2018)
787 1174. 10.1186/s12885-018-5080-4.

788 [11] K.P. Huang, A.A. Acosta, M.Y. Ghidewon, A.D. McKnight, M.S. Almeida, N.T. Nyema, et
789 al., Dissociable hindbrain GLP1R circuits for satiety and aversion, Nature. 632 (2024) 585-93.
790 10.1038/s41586-024-07685-6.

791 [12] W. Cheng, D. Gordian, M.Q. Ludwig, T.H. Pers, R.J. Seeley, M.G. Myers, Jr., Hindbrain
792 circuits in the control of eating behaviour and energy balance, Nat Metab. 4 (2022) 826-35.
793 10.1038/s42255-022-00606-9.

794 [13] M.M. Veniant, S.C. Lu, L. Atangan, R. Komorowski, S. Stanislaus, Y. Cheng, et al., A GIPR
795 antagonist conjugated to GLP-1 analogues promotes weight loss with improved metabolic
796 parameters in preclinical and phase 1 settings, Nat Metab. 6 (2024) 290-303. 10.1038/s42255-
797 023-00966-w.

798 [14] J.M. Adams, H. Pei, D.A. Sandoval, R.J. Seeley, R.B. Chang, S.D. Liberles, et al.,
799 Liraglutide Modulates Appetite and Body Weight Through Glucagon-Like Peptide 1 Receptor-
800 Expressing Glutamatergic Neurons, Diabetes. 67 (2018) 1538-48. 10.2337/db17-1385.

801 [15] I. Medic, S. Gulati, H.-J. Lenz, D. Mahalingam, J. Thomas, J. Luo, et al., Initial results of a
802 cohort of advanced prostate cancer patients in a phase Ia study of NGM120, a first-in-class
803 anti- GDNF family receptor alpha like (GFRAL) antibody, Annals of Oncology. 33 (2022) S1186-
804 S. 10.1016/j.annonc.2022.07.1888.

805 [16] L. Yang, C.C. Chang, Z. Sun, D. Madsen, H. Zhu, S.B. Padkjaer, et al., GFRAL is the
806 receptor for GDF15 and is required for the anti-obesity effects of the ligand, Nat Med. 23 (2017)
807 1158-66. https://doi.org/10.1038/nm.4394.

808 [17] C.W. Roman, V.A. Derkach, R.D. Palmiter, Genetically and functionally defined NTS to PBN
809 brain circuits mediating anorexia, Nat Commun. 7 (2016) 11905. 10.1038/ncomms11905.

810 [18] G.K.C. Dowsett, B.Y.H. Lam, J.A. Tadross, I. Cimino, D. Rimmington, A.P. Coll, et al., A
811 survey of the mouse hindbrain in the fed and fasted states using single-nucleus RNA
812 sequencing, Mol Metab. 53 (2021) 101240. 10.1016/j.molmet.2021.101240.

813 [19] C. Zhang, J.A. Kaye, Z. Cai, Y. Wang, S.L. Prescott, S.D. Liberles, Area Postrema Cell
814 Types that Mediate Nausea-Associated Behaviors, Neuron. 109 (2021) 461-72 e5.
815 10.1016/j.neuron.2020.11.010.

816 [20] S.M. Fortin, R.K. Lipsky, R. Lhamo, J. Chen, E. Kim, T. Borner, et al., GABA neurons in the
817 nucleus tractus solitarius express GLP-1 receptors and mediate anorectic effects of liraglutide in
818 rats, Sci Transl Med. 12 (2020) 10.1126/scitranslmed.aay8071.

819 [21] G.X. Zheng, J.M. Terry, P. Belgrader, P. Ryvkin, Z.W. Bent, R. Wilson, et al., Massively
820 parallel digital transcriptional profiling of single cells, Nat Commun. 8 (2017) 14049.
821 10.1038/ncomms14049.

822 [22] R.C. Team. R: A Language and Environment for Statistical Computing. Vienna, Austria: R
823 Foundation for Statistical Computing; 2023.

824 [23] Y. Hao, T. Stuart, M.H. Kowalski, S. Choudhary, P. Hoffman, A. Hartman, et al., Dictionary
825 learning for integrative, multimodal and scalable single-cell analysis, Nat Biotechnol. 42 (2024)
826 293-304. 10.1038/s41587-023-01767-y.

827 [24] C.S. McGinnis, L.M. Murrow, Z.J. Gartner, DoubletFinder: Doublet Detection in Single-Cell
828 RNA Sequencing Data Using Artificial Nearest Neighbors, Cell Syst. 8 (2019) 329-37 e4.
829 10.1016/j.cels.2019.03.003.

830 [25] I. Korsunsky, N. Millard, J. Fan, K. Slowikowski, F. Zhang, K. Wei, et al., Fast, sensitive and
831 accurate integration of single-cell data with Harmony, Nat Methods. 16 (2019) 1289-96.
832 https://doi.org/10.1038/s41592-019-0619-0.

833 [26] J.N. Campbell, E.Z. Macosko, H. Fenselau, T.H. Pers, A. Lyubetskaya, D. Tenen, et al., A
834 molecular census of arcuate hypothalamus and median eminence cell types, Nat Neurosci. 20
835 (2017) 484-96. 10.1038/nn.4495.

836 [27] R. Chen, X. Wu, L. Jiang, Y. Zhang, Single-Cell RNA-Seq Reveals Hypothalamic Cell
837 Diversity, Cell Rep. 18 (2017) 3227-41. 10.1016/j.celrep.2017.03.004.

838 [28] R.A. Romanov, A. Zeisel, J. Bakker, F. Girach, A. Hellysaz, R. Tomer, et al., Molecular
839 interrogation of hypothalamic organization reveals distinct dopamine neuronal subtypes, Nat
840 Neurosci. 20 (2017) 176-88. 10.1038/nn.4462.

841 [29] B. Tasic, V. Menon, T.N. Nguyen, T.K. Kim, T. Jarsky, Z. Yao, et al., Adult mouse cortical
842 cell taxonomy revealed by single cell transcriptomics, Nat Neurosci. 19 (2016) 335-46.
843 10.1038/nn.4216.

844 [30] D. Aran, A.P. Looney, L. Liu, E. Wu, V. Fong, A. Hsu, et al., Reference-based analysis of
845 lung single-cell sequencing reveals a transitional profibrotic macrophage, Nat Immunol. 20
846 (2019) 163-72. https://doi.org/10.1038/s41590-018-0276-y.

847 [31] D. Risso, M. Cole. scRNAseq: Collection of Public Single-Cell RNA-Seq Datasets. 2.16.0
848 ed2023.

849 [32] G. Finak, A. McDavid, M. Yajima, J. Deng, V. Gersuk, A.K. Shalek, et al., MAST: a flexible
850 statistical framework for assessing transcriptional changes and characterizing heterogeneity in
851 single-cell RNA sequencing data, Genome Biol. 16 (2015) 278. 10.1186/s13059-015-0844-5.

852 [33] R. Cannoodt, W. Saelens, D. Sichien, S. Tavernier, S. Janssens, M. Guilliams, et al.,
853 SCORPIUS improves trajectory inference and identifies novel modules in dendritic cell
854 development., Preprint at bioRxiv. (2016) https://doi.org/10.1101/079509.

855 [34] K. Ushey, J. Allaire, Y. Tang. reticulate: Interface to 'Python'. 1.35.0 ed2024.

856 [35] R. Cannoodt. anndata: 'anndata' for R. 0.7.5.6 ed2023.

857 [36] G. Van Rossum, F.L. Drake. Python 3 Reference Manual. 3.9 ed. Scotts Valley, CA:
858 CreateSpace; 2009.

859 [37] A. Sathyamurthy, K.R. Johnson, K.J.E. Matson, C.I. Dobrott, L. Li, A.R. Ryba, et al.,
860 Massively Parallel Single Nucleus Transcriptional Profiling Defines Spinal Cord Neurons and
861 Their Activity during Behavior, Cell Rep. 22 (2018) 2216-25. 10.1016/j.celrep.2018.02.003.

862 [38] M.Y. Batiuk, A. Martirosyan, J. Wahis, F. de Vin, C. Marneffe, C. Kusserow, et al.,
863 Identification of region-specific astrocyte subtypes at single cell resolution, Nat Commun. 11
864 (2020) 1220. 10.1038/s41467-019-14198-8.

865 [39] L. Michielsen, M. Lotfollahi, D. Strobl, L. Sikkema, M.J.T. Reinders, F.J. Theis, et al., Single-
866 cell reference mapping to construct and extend cell-type hierarchies, NAR Genom Bioinform. 5
867 (2023) lqad070. 10.1093/nargab/lqad070.

868 [40] A. Gayoso, R. Lopez, G. Xing, P. Boyeau, V. Valiollah Pour Amiri, J. Hong, et al., A Python
869 library for probabilistic analysis of single-cell omics data, Nat Biotechnol. 40 (2022) 163-6.
870 10.1038/s41587-021-01206-w.

871 [41] L. Michielsen, M.J.T. Reinders, A. Mahfouz, Hierarchical progressive learning of cell
872 identities in single-cell data, Nat Commun. 12 (2021) 2799. 10.1038/s41467-021-23196-8.

873 [42] J.D. Hunter, Matplotlib: A 2D graphics environment, Computing in Science & Engineering.
874 3 (2007) 90-5. 10.1109/MCSE.2007.55.

875 [43] L. Steuernagel, B.Y.H. Lam, P. Klemm, G.K.C. Dowsett, C.A. Bauder, J.A. Tadross, et al.,
876 HypoMap-a unified single-cell gene expression atlas of the murine hypothalamus, Nat Metab. 4
877 (2022) 1402-19. 10.1038/s42255-022-00657-y.

878 [44] S. Jessa, A. Blanchet-Cohen, B. Krug, M. Vladoiu, M. Coutelier, D. Faury, et al., Stalled
879 developmental programs at the root of pediatric brain tumors, Nat Genet. 51 (2019) 1702-13.
880 10.1038/s41588-019-0531-7.

881 [45] C.E. Vaaga, M. Borisovska, G.L. Westbrook, Dual-transmitter neurons: functional
882 implications of co-release and co-transmission, Curr Opin Neurobiol. 29 (2014) 25-32.
883 10.1016/j.conb.2014.04.010.

884 [46] N.X. Tritsch, A.J. Granger, B.L. Sabatini, Mechanisms and functions of GABA co-release,
885 Nat Rev Neurosci. 17 (2016) 139-45. 10.1038/nrn.2015.21.

886 [47] C.F. Landry, J.A. Ellison, T.M. Pribyl, C. Campagnoni, K. Kampf, A.T. Campagnoni, Myelin
887 basic protein gene expression in neurons: developmental and regional changes in protein
888 targeting within neuronal nuclei, cell bodies, and processes., J Neurosci. 16 (1996) 2452-62.
889 10.1523/JNEUROSCI.16-08-02452.1996.

890 [48] D. Lutz, G. Loers, R. Kleene, I. Oezen, H. Kataria, N. Katagihallimath, et al., Myelin basic
891 protein cleaves cell adhesion molecule L1 and promotes neuritogenesis and cell survival, J Biol
892 Chem. 289 (2014) 13503-18. 10.1074/jbc.M113.530238.

893 [49] V.T. Cheli, D.A. Santiago Gonzalez, V. Spreuer, V. Handley, A.T. Campagnoni, P.M. Paez,
894 Golli Myelin Basic Proteins Modulate Voltage-Operated Ca(++) Influx and Development in
895 Cortical and Hippocampal Neurons, Mol Neurobiol. 53 (2016) 5749-71. 10.1007/s12035-015-
896 9499-1.

897 [50] M. Melone, S. Ciappelloni, F. Conti, Plasma membrane transporters GAT-1 and GAT-3
898 contribute to heterogeneity of GABAergic synapses in neocortex, Front Neuroanat. 8 (2014) 72.
899 10.3389/fnana.2014.00072.

900 [51] S.M. Theparambil, P.S. Hosford, I. Ruminot, O. Kopach, J.R. Reynolds, P.Y. Sandoval, et
901 al., Astrocytes regulate brain extracellular pH via a neuronal activity-dependent bicarbonate
902 shuttle, Nat Commun. 11 (2020) 5073. 10.1038/s41467-020-18756-3.

903 [52] Y. Kubo, T.J. Baldwin, Y.N. Jan, L.Y. Jan, Primary structure and functional expression of a
904 mouse inward rectifier potassium channel, Nature. 362 (1993) 127–33.
905 https://doi.org/10.1038/362127a0.

906 [53] N. Burnashev, A. Khodorova, P. Jonas, P.J. Helm, W. Wisden, H. Monyer, et al., Calcium-
907 Permeable AMPA-Kainate Receptors in Fusiform Cerebellar Glial Cells, Science. 256 (1992)
908 1566-70. http://dx.doi.org/10.1126/science.1317970.

909 [54] J.R.P. Geiger, T. Melcher, D.S. Koh, B. Sakmann, S.P. H., P. Jonas, et al., Relative
910 Abundance of Subunit mRNAs Determines Gating and Ca*+ Permeability of AMPA Receptors in
911 Principal Neurons and Interneurons in Rat CNS, Neuron. 15 (1995) 193-204.
912 doi:10.1016/0896-6273(95)90076-4.

913 [55] S. Marques, A. Zeisel, S. Codeluppi, D. van Bruggen, A. Mendanha Falcao, L. Xiao, et al.,
914 Oligodendrocyte heterogeneity in the mouse juvenile and adult central nervous system,
915 Science. 352 (2016) 1326-9. 10.1126/science.aaf6463.

916 [56] M. Kasai, Y. Omae, Y. Kawai, A. Shibata, A. Hoshino, M. Mizuguchi, et al., GWAS identifies
917 candidate susceptibility loci and microRNA biomarkers for acute encephalopathy with biphasic
918 seizures and late reduced diffusion, Sci Rep. 12 (2022) 1332. 10.1038/s41598-021-04576-y.

919 [57] A.B. DePaula-Silva, C. Gorbea, D.J. Doty, J.E. Libbey, J.M.S. Sanchez, T.J. Hanak, et al.,
920 Differential transcriptional profiles identify microglial- and macrophage-specific gene markers
921 expressed during virus-induced neuroinflammation, J Neuroinflammation. 16 (2019) 152.
922 10.1186/s12974-019-1545-x.

923 [58] N. Koutsodendris, J. Blumenfeld, A. Agrawal, M. Traglia, B. Grone, M. Zilberter, et al.,
924 Neuronal APOE4 removal protects against tau-mediated gliosis, neurodegeneration and myelin
925 deficits, Nat Aging. 3 (2023) 275-96. 10.1038/s43587-023-00368-3.

926 [59] L. Schirmer, D. Velmeshev, S. Holmqvist, M. Kaufmann, S. Werneburg, D. Jung, et al.,
927 Neuronal vulnerability and multilineage diversity in multiple sclerosis, Nature. 573 (2019) 75-82.
928 10.1038/s41586-019-1404-z.

929 [60] J. Creus-Muncunill, J.V. Haure-Mirande, D. Mattei, J. Bons, A.V. Ramirez, B.W. Hamilton,
930 et al., TYROBP/DAP12 knockout in Huntington's disease Q175 mice cell-autonomously
931 decreases microglial expression of disease-associated genes and non-cell-autonomously
932 mitigates astrogliosis and motor deterioration, J Neuroinflammation. 21 (2024) 66.
933 10.1186/s12974-024-03052-4.

934 [61] L.L. Tang, Y.B. Wu, C.Q. Fang, P. Qu, Z.L. Gao, NDRG2 promoted secreted miR-375 in
935 microvesicles shed from M1 microglia, which induced neuron damage, Biochem Biophys Res
936 Commun. 469 (2016) 392-8. 10.1016/j.bbrc.2015.11.098.

937 [62] W. Cheng, E. Ndoka, C. Hutch, K. Roelofs, A. MacKinnon, B. Khoury, et al., Leptin
938 receptor-expressing nucleus tractus solitarius neurons suppress food intake independently of
939 GLP1 in mice, JCI Insight. 5 (2020) 10.1172/jci.insight.134359.

940 [63] C.W. Roman, S.R. Sloat, R.D. Palmiter, A tale of two circuits: CCK(NTS) neuron stimulation
941 controls appetite and induces opposing motivational states by projections to distinct brain
942 regions, Neuroscience. 358 (2017) 316-24. 10.1016/j.neuroscience.2017.06.049.

943 [64] V. Chou, R.V. Pearse, 2nd, A.J. Aylward, N. Ashour, M. Taga, G. Terzioglu, et al., INPP5D
944 regulates inflammasome activation in human microglia, Nat Commun. 14 (2023) 7552.
945 10.1038/s41467-023-42819-w.

946 [65] S.O. Kleeman, T.M. Thakir, B. Demestichas, N. Mourikis, D. Loiero, M. Ferrer, et al.,
947 Cystatin C is glucocorticoid responsive, directs recruitment of Trem2+ macrophages, and
948 predicts failure of cancer immunotherapy, Cell Genom. 3 (2023) 100347.
949 10.1016/j.xgen.2023.100347.

950 [66] S.H. Kang, M. Fukaya, J.K. Yang, J.D. Rothstein, D.E. Bergles, NG2+ CNS glial progenitors
951 remain committed to the oligodendrocyte lineage in postnatal life and following
952 neurodegeneration, Neuron. 68 (2010) 668-81. 10.1016/j.neuron.2010.09.009.

953 [67] T.P. Bachor, E. Hwang, E. Yulyaningsih, K. Attal, F. Mifsud, V. Pham, et al., Identification of
954 AgRP cells in the murine hindbrain that drive feeding, Mol Metab. 80 (2024) 101886.
955 10.1016/j.molmet.2024.101886.

956 [68] M.K. Holt, The ins and outs of the caudal nucleus of the solitary tract: An overview of
957 cellular populations and anatomical connections, J Neuroendocrinol. 34 (2022) e13132.
958 10.1111/jne.13132.

959 [69] D.M. Breen, H. Kim, D. Bennett, R.A. Calle, S. Collins, R.M. Esquejo, et al., GDF-15
960 Neutralization Alleviates Platinum-Based Chemotherapy-Induced Emesis, Anorexia, and Weight
961 Loss in Mice and Nonhuman Primates, Cell Metab. 32 (2020) 938-50 e6.
962 10.1016/j.cmet.2020.10.023.

963 [70] K. Tsuzuki, S. Ishiuchi, GluR2 expressed by glial fibrillary acidic protein promoter decreases
964 the number of neurons, Front Biosci (Landmark Ed). 13 (2008) 2784–96.
965 https://doi.org/10.2741/2885.

966 [71] F. Endo, A. Kasai, J.S. Soto, X. Yu, Z. Qu, H. Hashimoto, et al., Molecular basis of
967 astrocyte diversity and morphology across the CNS in health and disease, Science. 378 (2022)
968 eadc9020. 10.1126/science.adc9020.

969 [72] R. Lujan, Organisation of potassium channels on the neuronal surface, J Chem Neuroanat.
970 40 (2010) 1-20. 10.1016/j.jchemneu.2010.03.003.

971 [73] R. Cabezas, M. Avila, J. Gonzalez, R.S. El-Bacha, E. Baez, L.M. Garcia-Segura, et al.,
972 Astrocytic modulation of blood brain barrier: perspectives on Parkinson's disease, Front Cell
973 Neurosci. 8 (2014) 211. 10.3389/fncel.2014.00211.

974 [74] W. Cheng, I. Gonzalez, W. Pan, A.H. Tsang, J. Adams, E. Ndoka, et al., Calcitonin
975 Receptor Neurons in the Mouse Nucleus Tractus Solitarius Control Energy Balance via the Non-
976 aversive Suppression of Feeding, Cell Metab. 31 (2020) 301-12 e5.
977 10.1016/j.cmet.2019.12.012.

978 [75] A.R. Patel, H. Frikke-Schmidt, P.V. Sabatini, A.C. Rupp, D.A. Sandoval, M.G. Myers, Jr., et
979 al., Neither GLP-1 receptors nor GFRAL neurons are required for aversive or anorectic
980 response to DON (vomitoxin), Am J Physiol Regul Integr Comp Physiol. 324 (2023) R635-44.
981 10.1152/ajpregu.00189.2022.

982 [76] S.C. Robins, E. Trudel, O. Rotondi, X. Liu, T. Djogo, D. Kryzskaya, et al., Evidence for NG2-
983 glia derived, adult-born functional neurons in the hypothalamus, PLoS One. 8 (2013) e78236.
984 10.1371/journal.pone.0078236.

985 [77] C.G. Liberini, T. Borner, C.N. Boyle, T.A. Lutz, The satiating hormone amylin enhances
986 neurogenesis in the area postrema of adult rats, Mol Metab. 5 (2016) 834-43.
987 10.1016/j.molmet.2016.06.015.

988 [78] N. Wada, S. Hirako, F. Takenoya, H. Kageyama, M. Okabe, S. Shioda, Leptin and its
989 receptors, J Chem Neuroanat. 61-62 (2014) 191-9. 10.1016/j.jchemneu.2014.09.002.

990 [79] H. Munzberg, J.S. Flier, C. Bjorbaek, Region-specific leptin resistance within the
991 hypothalamus of diet-induced obese mice, Endocrinology. 145 (2004) 4880-9.
992 10.1210/en.2004-0726.

993 [80] P.M. Smith, P. Brzezinska, F. Hubert, A. Mimee, D.H. Maurice, A.V. Ferguson, Leptin
994 influences the excitability of area postrema neurons, Am J Physiol Regul Integr Comp Physiol.
995 310 (2016) R440-8. 10.1152/ajpregu.00326.2015.

996 [81] C.G. Liberini, C.N. Boyle, C. Cifani, M. Venniro, B.T. Hope, T.A. Lutz, Amylin receptor
997 components and the leptin receptor are co-expressed in single rat area postrema neurons, Eur
998 J Neurosci. 43 (2016) 653-61. 10.1111/ejn.13163.

999 [82] L. Huo, L. Maeng, C. Bjorbaek, H.J. Grill, Leptin and the control of food intake: neurons in
1000 the nucleus of the solitary tract are activated by both gastric distension and leptin,
1001 Endocrinology. 148 (2007) 2189-97. 10.1210/en.2006-1572.

1002 [83] J.P.H. Wilding, R.L. Batterham, S. Calanna, M. Davies, L.F. Van Gaal, I. Lingvay, et al.,
1003 Once-Weekly Semaglutide in Adults with Overweight or Obesity, N Engl J Med. 384 (2021) 989-
1004 1002. 10.1056/NEJMoa2032183.

1005 [84] B.B. Lake, R. Ai, G.E. Kaeser, N.S. Salathia, Y.C. Yung, R. Liu, et al., Neuronal subtypes
1006 and diversity revealed by single-nucleus RNA sequencing of the human brain, Science. 352
1007 (2016) 1586-90. 10.1126/science.aaf1204.

1008 [85] B.B. Lake, S. Codeluppi, Y.C. Yung, D. Gao, J. Chun, P.V. Kharchenko, et al., A
1009 comparative strategy for single-nucleus and single-cell transcriptomes confirms accuracy in
1010 predicted cell-type expression from nuclear RNA, Sci Rep. 7 (2017) 6031. 10.1038/s41598-
1011 017-04426-w.

1012 [86] N. Thrupp, C. Sala Frigerio, L. Wolfs, N.G. Skene, N. Fattorelli, S. Poovathingal, et al.,
1013 Single-Nucleus RNA-Seq Is Not Suitable for Detection of Microglial Activation Genes in Humans,
1014 Cell Rep. 32 (2020) 108189. 10.1016/j.celrep.2020.108189.

1015 [87] H. Thorvaldsdottir, J.T. Robinson, J.P. Mesirov, Integrative Genomics Viewer (IGV): high-
1016 performance genomics data visualization and exploration, Brief Bioinform. 14 (2013) 178-92.
1017 10.1093/bib/bbs017.

1018 [88] M.J. Park, K. Chung, Endogenous lectin (RL-29) expression of the autonomic preganglionic
1019 neurons in the rat spinal cord, The Anatomical Record. 254 (1999) 54-60.
1020 10.1002/%28SICI%291097-0185%2819990101%29254%3A1%3C53%3A%3AAID-
1021 AR7%3E3.0.CO%3B2-H.

1022 [89] C.O. Miranda, K. Hegedus, H. Wildner, H.U. Zeilhofer, M. Antal, Morphological and
1023 neurochemical characterization of glycinergic neurons in laminae I-IV of the mouse spinal dorsal
1024 horn, J Comp Neurol. 530 (2022) 607-26. 10.1002/cne.25232.

1025 [90] F. Guo, Y. Wang, TCF7l2, a nuclear marker that labels premyelinating oligodendrocytes and
1026 promotes oligodendroglial lineage progression, Glia. 71 (2023) 143-54. 10.1002/glia.24249.

1027 [91] E. Weihe, C. Depboylu, B. Schutz, M.K. Schafer, L.E. Eiden, Three types of tyrosine
1028 hydroxylase-positive CNS neurons distinguished by dopa decarboxylase and VMAT2 co-
1029 expression, Cell Mol Neurobiol. 26 (2006) 659-78. 10.1007/s10571-006-9053-9.

1030 [92] J. Sun, Y. Song, Z. Chen, J. Qiu, S. Zhu, L. Wu, et al., Heterogeneity and Molecular Markers
1031 for CNS Glial Cells Revealed by Single-Cell Transcriptomics, Cell Mol Neurobiol. 42 (2022) 2629-
1032 42. 10.1007/s10571-021-01159-3.

1033 [93] M. Dallaporta, M.S. Bonnet, K. Horner, J. Trouslard, A. Jean, J.D. Troadec, Glial cells of the
1034 nucleus tractus solitarius as partners of the dorsal hindbrain regulation of energy balance: a
1035 proposal for a working hypothesis, Brain Res. 1350 (2010) 35-42.
1036 10.1016/j.brainres.2010.04.025.

1037 [94] J. Kalucka, L. de Rooij, J. Goveia, K. Rohlenova, S.J. Dumas, E. Meta, et al., Single-Cell
1038 Transcriptome Atlas of Murine Endothelial Cells, Cell. 180 (2020) 764-79 e20.
1039 10.1016/j.cell.2020.01.015.

1040 [95] N. Dani, R.H. Herbst, C. McCabe, G.S. Green, K. Kaiser, J.P. Head, et al., A cellular and
1041 spatial map of the choroid plexus across brain ventricles and ages, Cell. 184 (2021) 3056-74 e21.
1042 10.1016/j.cell.2021.04.003.

1043 [96] B. Ray, J.A. Bailey, S. Sarkar, D.K. Lahiri, Molecular and immunocytochemical
1044 characterization of primary neuronal cultures from adult rat brain: Differential expression of
1045 neuronal and glial protein markers, J Neurosci Methods. 184 (2009) 294-302.
1046 10.1016/j.jneumeth.2009.08.018.

1047 [97] S.E. Lauri, M. Ryazantseva, E. Orav, A. Vesikansa, T. Taira, Kainate receptors in the
1048 developing neuronal networks, Neuropharmacology. 195 (2021) 108585.
1049 10.1016/j.neuropharm.2021.108585.

1050 [98] Y.H. Song, J. Yoon, S.H. Lee, The role of neuropeptide somatostatin in the brain and its
1051 application in treating neurological disorders, Exp Mol Med. 53 (2021) 328-38. 10.1038/s12276-
1052 021-00580-4.

1053 [99] H.W. Song, K.L. Foreman, B.D. Gastfriend, J.S. Kuo, S.P. Palecek, E.V. Shusta,
1054 Transcriptomic comparison of human and mouse brain microvessels, Sci Rep. 10 (2020) 12358.
1055 10.1038/s41598-020-69096-7.

1056 [100] L. Xu, Y. Yao, Central Nervous System Fibroblast-Like Cells in Stroke and Other
1057 Neurological Disorders, Stroke. 52 (2021) 2456-64. 10.1161/STROKEAHA.120.033431.

1058 [101] U. Ernsberger, H. Rohrer, Sympathetic tales: subdivisons of the autonomic nervous system
1059 and the impact of developmental studies, Neural Dev. 13 (2018) 20. 10.1186/s13064-018-0117-
1060 6.

1061 [102] C.R. Gajera, H. Emich, O. Lioubinski, A. Christ, R. Beckervordersandforth-Bonk, K.
1062 Yoshikawa, et al., LRP2 in ependymal cells regulates BMP signaling in the adult neurogenic niche,
1063 J Cell Sci. 123 (2010) 1922-30. 10.1242/jcs.065912.

1064 [103] A. MacDonald, B. Lu, M. Caron, N. Caporicci-Dinucci, D. Hatrock, K. Petrecca, et al., Single
1065 Cell Transcriptomics of Ependymal Cells Across Age, Region and Species Reveals Cilia-Related
1066 and Metal Ion Regulatory Roles as Major Conserved Ependymal Cell Functions, Front Cell
1067 Neurosci. 15 (2021) 703951. 10.3389/fncel.2021.703951.

1068 [104] H.W. Jeong, R. Dieguez-Hurtado, H. Arf, J. Song, H. Park, K. Kruse, et al., Single-cell
1069 transcriptomics reveals functionally specialized vascular endothelium in brain, Elife. 11 (2022)
1070 10.7554/eLife.57520.

1071 [105] K. Huizer, D.A.M. Mustafa, J.C. Spelt, J.M. Kros, A. Sacchetti, Improving the
1072 characterization of endothelial progenitor cell subsets by an optimized FACS protocol, PLoS One.
1073 12 (2017) e0184895. 10.1371/journal.pone.0184895.

1074 [106] E. Gerrits, Y. Heng, E. Boddeke, B.J.L. Eggen, Transcriptional profiling of microglia; current
1075 state of the art and future perspectives, Glia. 68 (2020) 740-55. 10.1002/glia.23767.

1076 [107] P.T. Shah, J.A. Stratton, M.G. Stykel, S. Abbasi, S. Sharma, K.A. Mayr, et al., Single-Cell
1077 Transcriptomics and Fate Mapping of Ependymal Cells Reveals an Absence of Neural Stem Cell
1078 Function, Cell. 173 (2018) 1045-57 e9. 10.1016/j.cell.2018.03.063.

1079 [108] C.G. Causing, A. Gloster, R. Aloyz, S.X. Bamji, E. Chang, J. Fawcett, et al., Synaptic
1080 Innervation Density Is Regulated by Neuron-Derived BDNF, Neuron. 18 (1997) 257–67.
1081 https://www.cell.com/fulltext/S0896-6273(00)80266-4#secd33944447e474.

1082 [109] Y. Zhang, S.A. Sloan, L.E. Clarke, C. Caneda, C.A. Plaza, P.D. Blumenthal, et al.,
1083 Purification and Characterization of Progenitor and Mature Human Astrocytes Reveals

1084 Transcriptional and Functional Differences with Mouse, Neuron. 89 (2016) 37-53.
1085 10.1016/j.neuron.2015.11.013.

1086 [110] F. Langlet, Tanycyte Gene Expression Dynamics in the Regulation of Energy Homeostasis,
1087 Front Endocrinol (Lausanne). 10 (2019) 286. 10.3389/fendo.2019.00286.

1088 [111] O. Uriarte Huarte, D. Kyriakis, T. Heurtaux, Y. Pires-Afonso, K. Grzyb, R. Halder, et al.,
1089 Single-Cell Transcriptomics and In Situ Morphological Analyses Reveal Microglia Heterogeneity
1090 Across the Nigrostriatal Pathway, Front Immunol. 12 (2021) 639613.
1091 10.3389/fimmu.2021.639613.

1092 [112] R.E. Pepper, K.A. Pitman, C.L. Cullen, K.M. Young, How Do Cells of the Oligodendrocyte
1093 Lineage Affect Neuronal Circuits to Influence Motor Function, Memory and Mood?, Front Cell
1094 Neurosci. 12 (2018) 399. 10.3389/fncel.2018.00399.

1095 [113] A. Maegawa, K. Murata, K. Kuroda, S. Fujieda, Y. Fukazawa, Cellular Profiles of
1096 Prodynorphin and Preproenkephalin mRNA-Expressing Neurons in the Anterior Olfactory
1097 Tubercle of Mice, Front Neural Circuits. 16 (2022) 908964. 10.3389/fncir.2022.908964.

1098 [114] S.T. Hentges, V. Otero-Corchon, R.L. Pennock, C.M. King, M.J. Low, Proopiomelanocortin
1099 expression in both GABA and glutamate neurons, J Neurosci. 29 (2009) 13684-90.
1100 10.1523/JNEUROSCI.3770-09.2009.

1101 [115] W. Sun, A. Cornwell, J. Li, S. Peng, M.J. Osorio, N. Aalling, et al., SOX9 Is an Astrocyte-
1102 Specific Nuclear Marker in the Adult Brain Outside the Neurogenic Regions, J Neurosci. 37 (2017)
1103 4493-507. 10.1523/JNEUROSCI.3199-16.2017.

1104 [116] A.T. Lee, D. Vogt, J.L. Rubenstein, V.S. Sohal, A class of GABAergic neurons in the
1105 prefrontal cortex sends long-range projections to the nucleus accumbens and elicits acute
1106 avoidance behavior, J Neurosci. 34 (2014) 11519-25. 10.1523/JNEUROSCI.1157-14.2014.

1107 [117] M. Vanlandewijck, L. He, M.A. Mae, J. Andrae, K. Ando, F. Del Gaudio, et al., A molecular
1108 atlas of cell types and zonation in the brain vasculature, Nature. 554 (2018) 475-80.
1109 10.1038/nature25739.

1110 [118] M. Carlen, K. Meletis, C. Goritz, V. Darsalia, E. Evergren, K. Tanigaki, et al., Forebrain
1111 ependymal cells are Notch-dependent and generate neuroblasts and astrocytes after stroke, Nat
1112 Neurosci. 12 (2009) 259-67. 10.1038/nn.2268.

1113 [119] J. Garcia-Revilla, A. Boza-Serrano, A.M. Espinosa-Oliva, M.S. Soto, T. Deierborg, R. Ruiz,
1114 et al., Galectin-3, a rising star in modulating microglia activation under conditions of
1115 neurodegeneration, Cell Death Dis. 13 (2022) 628. 10.1038/s41419-022-05058-3.

1116 [120] A.C. Yang, R.T. Vest, F. Kern, D.P. Lee, M. Agam, C.A. Maat, et al., A human brain vascular
1117 atlas reveals diverse mediators of Alzheimer's risk, Nature. 603 (2022) 885-92. 10.1038/s41586-
1118 021-04369-3.

1119 [121] S. Chasseigneaux, Y. Moraca, V. Cochois-Guegan, A.C. Boulay, A. Gilbert, S. Le Crom, et
1120 al., Isolation and differential transcriptome of vascular smooth muscle cells and mid-capillary
1121 pericytes from the rat brain, Sci Rep. 8 (2018) 12272. 10.1038/s41598-018-30739-5.

1122 [122] Z. Gao, K. Ure, J.L. Ables, D.C. Lagace, K.A. Nave, S. Goebbels, et al., Neurod1 is essential
1123 for the survival and maturation of adult-born neurons, Nat Neurosci. 12 (2009) 1090-2.
1124 10.1038/nn.2385.

1125 [123] T. Kodama, S. Guerrero, M. Shin, S. Moghadam, M. Faulstich, S. du Lac, Neuronal
1126 classification and marker gene identification via single-cell expression profiling of brainstem
1127 vestibular neurons subserving cerebellar learning, J Neurosci. 32 (2012) 7819-31.
1128 10.1523/JNEUROSCI.0543-12.2012.

1129 [124] J. Manjarrez-Marmolejo, J. Franco-Pérez, Gap Junction Blockers- An Overview of their
1130 Effects on Induced Seizures in Animal Models, Current Neuropharmacology. 14 (2016) 759-71.
1131 10.2174/1570159X14666160603115.

1132 [125] T. Paretkar, E. Dimitrov, Activation of enkephalinergic (Enk) interneurons in the central
1133 amygdala (CeA) buffers the behavioral effects of persistent pain, Neurobiol Dis. 124 (2019) 364-
1134 72. 10.1016/j.nbd.2018.12.005.

1135 [126] Z. Zhang, Z. Ma, W. Zou, H. Guo, M. Liu, Y. Ma, et al., The Appropriate Marker for
1136 Astrocytes: Comparing the Distribution and Expression of Three Astrocytic Markers in Different
1137 Mouse Cerebral Regions, Biomed Res Int. 2019 (2019) 9605265. 10.1155/2019/9605265.

1138 [127] A.M. Jurga, M. Paleczna, J. Kadluczka, K.Z. Kuter, Beyond the GFAP-Astrocyte Protein
1139 Markers in the Brain, Biomolecules. 11 (2021) 10.3390/biom11091361.

1140 [128] V. Dyachuk, A. Furlan, M.K. Shahidi, M. Giovenco, N. Kaukua, C. Konstantinidou, et al.,
1141 Parasympathetic neurons originate from nerve-associated peripheral glial progenitors, Science.
1142 345 (2014) 82-7. 10.1126/science.1253281.

1143 [129] D.S. Liu, T.L. Xu, Cell-Type Identification in the Autonomic Nervous System, Neurosci Bull.
1144 35 (2019) 145-55. 10.1007/s12264-018-0284-9.

1145 [130] B.J. Kang, D.A. Chang, D.D. Mackay, G.H. West, T.S. Moreira, A.C. Takakura, et al.,
1146 Central nervous system distribution of the transcription factor Phox2b in the adult rat, J Comp
1147 Neurol. 503 (2007) 627-41. 10.1002/cne.21409.

1148 [131] M. Adler, N. Moriel, A. Goeva, I. Avraham-Davidi, S. Mages, T.S. Adams, et al., Emergence
1149 of division of labor in tissues through cell interactions and spatial cues, Cell Rep. 42 (2023)
1150 112412. 10.1016/j.celrep.2023.112412.

1151 [132] A. Steimel, J. Suh, A. Hussainkhel, S. Deheshi, J.M. Grants, R. Zapf, et al., The C. elegans
1152 CDK8 Mediator module regulates axon guidance decisions in the ventral nerve cord and during
1153 dorsal axon navigation, Dev Biol. 377 (2013) 385-98. 10.1016/j.ydbio.2013.02.009.

1154 [133] T. Daiber, C.J. VanderZwan-Butler, G.J. Bashaw, T.A. Evans, Conserved and divergent
1155 aspects of Robo receptor signaling and regulation between Drosophila Robo1 and C. elegans
1156 SAX-3, Genetics. 217 (2021) 10.1093/genetics/iyab018.

1157 [134] S. Schmetsdorf, U. Gärtner, T. Arendt, Constitutive Expression of Functionally Active
1158 Cyclin-Dependent Kinases and Their Binding Partners Suggests Noncanonical Functions of Cell
1159 Cycle Regulators in Differentiated Neurons, Cerebral Cortex. 17 (2007) 1821–9.
1160 https://doi.org/10.1093/cercor/bhl091.

1161 [135] K.K. Kummer, M. Zeidler, T. Kalpachidou, M. Kress, Role of IL-6 in the regulation of neuronal
1162 development, survival and function, Cytokine. 144 (2021) 155582. 10.1016/j.cyto.2021.155582.

1163 [136] P. März, J.G. Cheng, R.A. Gadient, P.H. Patterson, T. Stoyan, U. Otten, et al., Sympathetic
1164 neurons can produce and respond to interleukin 6, Proc Natl Acad Sci. 95 (1998) 3251-6.
1165 10.1073/pnas.95.6.3251.

1166 [137] K.M. McGrail, J.M. Phillips, K.J. Sweadner, Immunofluorescent localization of three Na,K-
1167 ATPase isozymes in the rat central nervous system: both neurons and glia can express more than
1168 one Na,K-ATPase., J Neurosci. 11 (1991) 381-91. 10.1523/JNEUROSCI.11-02-00381.1991.

1169 [138] H. Poulsen, H. Khandelia, J.P. Morth, M. Bublitz, O.G. Mouritsen, J. Egebjerg, et al.,
1170 Neurological disease mutations compromise a C-terminal ion pathway in the Na(+)/K(+)-ATPase,
1171 Nature. 467 (2010) 99-102. 10.1038/nature09309.

1172 [139] A. Abousaab, J. Warsi, B. Elvira, F. Lang, Caveolin-1 Sensitivity of Excitatory Amino Acid
1173 Transporters EAAT1, EAAT2, EAAT3, and EAAT4, J Membr Biol. 249 (2016) 239-49.
1174 10.1007/s00232-015-9863-0.

1175 [140] E.R. Bongarzone, C.W. Campagnoni, K. Kampf, E.C. Jacobs, V.W. Handley, V.
1176 Schonmann, et al., Identification of a new exon in the myelin proteolipid protein gene encoding
1177 novel protein isoforms that are restricted to the somata of oligodendrocytes and neurons., J
1178 Neurosci. 19 (1999) 8349-57. 10.1523/JNEUROSCI.19-19-08349.

1179 [141] L.F. Nunnelly, M. Campbell, D.I. Lee, P. Dummer, G. Gu, V. Menon, et al., St18 specifies
1180 globus pallidus projection neuron identity in MGE lineage, Nat Commun. 13 (2022) 7735.
1181 10.1038/s41467-022-35518-5.

1182 [142] C. Plachez, C. Lindwall, N. Sunn, M. Piper, R.X. Moldrich, C.E. Campbell, et al., Nuclear
1183 factor I gene expression in the developing forebrain, J Comp Neurol. 508 (2008) 385-401.
1184 10.1002/cne.21645.

1185 [143] J. Fraser, A. Essebier, A.S. Brown, R.A. Davila, D. Harkins, O. Zalucki, et al., Common
1186 Regulatory Targets of NFIA, NFIX and NFIB during Postnatal Cerebellar Development,
1187 Cerebellum. 19 (2020) 89-101. 10.1007/s12311-019-01089-3.

1188 [144] L. Dubois , A. Vincent, The COE--Collier/Olf1/EBF--transcription factors: structural
1189 conservation and diversity of developmental functions, 108. 3-12 (2001) 10.1016/s0925-
1190 4773(01)00486-5.

1191 [145] Y. Liu, T. Lear, O. Iannone, S. Shiva, C. Corey, S. Rajbhandari, et al., The Proapoptotic F-
1192 box Protein Fbxl7 Regulates Mitochondrial Function by Mediating the Ubiquitylation and
1193 Proteasomal Degradation of Survivin, J Biol Chem. 290 (2015) 11843-52.
1194 10.1074/jbc.M114.629931.

1195 [146] H. Kim, N.C. Berens, N.E. Ochandarena, B.D. Philpot, Region and Cell Type Distribution of
1196 TCF4 in the Postnatal Mouse Brain, Front Neuroanat. 14 (2020) 42. 10.3389/fnana.2020.00042.

1197 [147] A. Sirp, A. Shubina, J. Tuvikene, L. Tamberg, C.S. Kiir, L. Kranich, et al., Expression of
1198 alternative transcription factor 4 mRNAs and protein isoforms in the developing and adult rodent
1199 and human tissues, Front Mol Neurosci. 15 (2022) 1033224. 10.3389/fnmol.2022.1033224.

1200 [148] R.D. Hodge, T.E. Bakken, J.A. Miller, K.A. Smith, E.R. Barkan, L.T. Graybuck, et al.,
1201 Conserved cell types with divergent features in human versus mouse cortex, Nature. 573 (2019)
1202 61-8. 10.1038/s41586-019-1506-7.

1203 [149] T. Kuroda, S. Yasuda, S. Tachi, S. Matsuyama, S. Kusakawa, K. Tano, et al., SALL3
1204 expression balance underlies lineage biases in human induced pluripotent stem cell
1205 differentiation, Nat Commun. 10 (2019) 2175. 10.1038/s41467-019-09511-4.

1206 [150] F. Morello, D. Borshagovski, M. Survila, L. Tikker, S. Sadik-Ogli, A. Kirjavainen, et al.,
1207 Molecular Fingerprint and Developmental Regulation of the Tegmental GABAergic and
1208 Glutamatergic Neurons Derived from the Anterior Hindbrain, Cell Rep. 33 (2020) 108268.
1209 10.1016/j.celrep.2020.108268.

1210 [151] L. Wolf, C.S. Gao, K. Gueta, Q. Xie, T. Chevallier, N.R. Podduturi, et al., Identification and
1211 characterization of FGF2-dependent mRNA: microRNA networks during lens fiber cell
1212 differentiation, G3 (Bethesda). 3 (2013) 2239-55. 10.1534/g3.113.008698.

1213 [152] H. Liu, M. Aramaki, Y. Fu, D. Forrest, Retinoid-Related Orphan Receptor beta and
1214 Transcriptional Control of Neuronal Differentiation, Curr Top Dev Biol. 125 (2017) 227-55.
1215 10.1016/bs.ctdb.2016.11.009.

1216 [153] M.G. Del Barrio, S. Bourane, K. Grossmann, R. Schule, S. Britsch, D.D. O'Leary, et al., A
1217 transcription factor code defines nine sensory interneuron subtypes in the mechanosensory area
1218 of the spinal cord, PLoS One. 8 (2013) e77928. 10.1371/journal.pone.0077928.

1219 [154] Y. Li, A. Osuma, E. Correa, M.A. Okebalama, P. Dao, O. Gaylord, et al., Establishment and
1220 maintenance of motor neuron identity via temporal modularity in terminal selector function, Elife.
1221 9 (2020) 10.7554/eLife.59464.

1222 [155] D. Moruzzo, L. Nobbio, B. Sterlini, G.G. Consalez, F. Benfenati, A. Schenone, et al., The
1223 Transcription Factors EBF1 and EBF2 Are Positive Regulators of Myelination in Schwann Cells,
1224 Mol Neurobiol. 54 (2017) 8117-27. 10.1007/s12035-016-0296-2.

1225 [156] M.A. Jimenez, P. Akerblad, M. Sigvardsson, E.D. Rosen, Critical role for Ebf1 and Ebf2 in
1226 the adipogenic transcriptional cascade, Mol Cell Biol. 27 (2007) 743-57. 10.1128/MCB.01557-
1227 06.

1228 [157] H. Yu, M. Rubinstein, M.J. Low, Developmental single-cell transcriptomics of hypothalamic
1229 POMC neurons reveal the genetic trajectories of multiple neuropeptidergic phenotypes, Elife. 11
1230 (2022) 10.7554/eLife.72883.

1231 [158] I. Singh, L. Wang, B. Xia, J. Liu, A. Tahiri, A. El Ouaamari, et al., Activation of arcuate
1232 nucleus glucagon-like peptide-1 receptor-expressing neurons suppresses food intake, Cell
1233 Biosci. 12 (2022) 178. 10.1186/s13578-022-00914-3.

1234 [159] L. Xiao, D.P. Merullo, T.M.I. Koch, M. Cao, M. Co, A. Kulkarni, et al., Expression of FoxP2
1235 in the basal ganglia regulates vocal motor sequences in the adult songbird, Nat Commun. 12
1236 (2021) 2617. 10.1038/s41467-021-22918-2.

1237 [160] T.T. Du, J.B. Dewey, E.L. Wagner, R. Cui, J. Heo, J.J. Park, et al., LMO7 deficiency reveals
1238 the significance of the cuticular plate for hearing function, Nat Commun. 10 (2019) 1117.
1239 10.1038/s41467-019-09074-4.

1240 [161] M.A. Wozniak, B.M. Baker, C.S. Chen, K.L. Wilson, The emerin-binding transcription factor
1241 Lmo7 is regulated by association with p130Cas at focal adhesions, PeerJ. 1 (2013) e134.
1242 10.7717/peerj.134.

1243 [162] T. Kawaue, A. Shitamukai, A. Nagasaka, Y. Tsunekawa, T. Shinoda, K. Saito, et al., Lzts1
1244 controls both neuronal delamination and outer radial glial-like cell generation during mammalian
1245 cerebral development, Nat Commun. 10 (2019) 2780. 10.1038/s41467-019-10730-y.

1246 [163] O. Randlett, L. Poggi, F.R. Zolessi, W.A. Harris, The oriented emergence of axons from
1247 retinal ganglion cells is directed by laminin contact in vivo, Neuron. 70 (2011) 266-80.
1248 10.1016/j.neuron.2011.03.013.

1249 [164] N. Ichikawa-Tomikawa, J. Ogawa, V. Douet, Z. Xu, Y. Kamikubo, T. Sakurai, et al., Laminin
1250 alpha1 is essential for mouse cerebellar development, Matrix Biol. 31 (2012) 17-28.
1251 10.1016/j.matbio.2011.09.002.

1252 [165] E.S. Liau, S. Jin, Y.C. Chen, W.S. Liu, M. Calon, S. Nedelec, et al., Single-cell transcriptomic
1253 analysis reveals diversity within mammalian spinal motor neurons, Nat Commun. 14 (2023) 46.
1254 10.1038/s41467-022-35574-x.
1255

1256 Figure legends

1257 Figure 1: Two layers of cell identity for the murine DVC cells from snRNA-seq data

1258 **A.** Adult C57BL/6J mice were subjected to 10X Genomics-based snRNA barcoding and
1259 sequencing after dissection of their DVC (n=30). **B.** Labeled UMAP plot of the mouse DVC (cells
1260 n=99,740) at the lowest resolution (layer 1) including 4 cell identities, and **C.** the cell class (layer
1261 2) including 18. **D.** Heatmap of the main marker genes (average log2FC expression >80
1262 percentiles of upregulated genes) for each neuronal class of the mouse DVC (MAST algorithm;
1263 neurons n= 48,131; adj. p<0.05). Each column is one cell and each row is one marker gene. **E.**
1264 Stacked barplot of log-normalized counts of genes for 10 transcripts (i.e. *Gad2*, *Gad1*, *Slc6a5*,
1265 *Slc17a6*, *Slc18a2*, *Addc*, *Sst*, *Npy*, *Cck* and *Slc5a7*) related to transmission/release of 8
1266 neurotransmitters and neuropeptides, by neuronal cell class. Each bar represents one neuron
1267 (n=48,131).

1268 snRNA-seq=single-nuclei RNA-sequencing; DVC=dorsal vagal complex; FACs=fluorescence-activated cell sorting;
1269 UMAP=uniform manifold approximation and projection; FC=fold-change; adj.=adjusted; GABA=gamma-aminobutyric
1270 acid

1271

1272 Figure 2: Third layer of non-neuronal murine DVC cell identities

1273 **A.** Labeled UMAP plot of the mouse DVC with the 15 non-neuronal cell identities shown (total
1274 cells n=99,740; non-neuronal cells n=51,609). **B.** UMAP plot showing scaled expression of *Gfap*,
1275 *Gria2* and *Kcnj3* genes in Ca^+-permeable astrocytes (circled; total cells n=99,740; Ca^+-permeable
1276 astrocytes n=1,719). **C.** Barplot of log-normalized expression of six genes in oligodendrocytes
1277 (premyelinating n=267; myelinating intermediate n=25,692; myelinating n= 6,170). Only
1278 premyelinating oligodendrocytes lack expression of *Mobp*, involved in myelin formation.
1279 Reduction of *Synpr* and *Opalin* expression is observed as *Anln* and *Aff3* increase in myelinating
1280 oligodendrocytes. **D.** Balloon plot of the main cell types of non-neuronal cells and neurons
1281 showing average log-normalized counts of their marker genes (MAST algorithm; adj. p<0.05).
1282 Markers shown are upregulated genes in >80% of cells per group with average log2FC>4, or
1283 upregulated in >70% of cells with average log2FC>8.

1284 DVC=dorsal vagal complex; UMAP=uniform manifold approximation and projection; APNTS=Area postrema and
1285 nucleus of the solitary tract; OL=oligodendrocyte; OPC=oligodendrocyte precursor cell; Smc=smooth muscle cells

1286

1287 Figure 3: Neuronal populations of the murine DVC

1288 **A.** Labeled UMAP plot with the neuronal layer 3 cell identities (neurons n=48,131). **B.** Monoamine
1289 class balloon plot showing average log-normalized expression of marker genes for each cell
1290 identity (MAST algorithm; M0 cells n=770, M1 cells n=551, M2 cells n=666 and M3 cells n=2,593;
1291 adj. $p<0.05$), and **C.** heatmap of expression of monoamine related genes. In the heatmap, each
1292 column represents one cell and each row, one gene. **D.** Barplot of *Gcg* average log-normalized
1293 expression by neuronal cell identity. **E.** UMAP plot showing the expression of leptin receptor and
1294 prolactin receptor genes in neurons. The GLP1 cluster is highlighted (GLP1 cells n=153). **F.**
1295 Stacked barplot of the proportion of cells expressing one or more GABA-related genes (i.e.
1296 *Slc32a1*, *Gad1*, *Gad2*) and glutamate-related genes (i.e. *Slc17a6*, *Slc17a7*). The proportion of
1297 cells per cell group co-expressing GABA and glutamate associated genes are shown in purple.
1298 Only cells with log-normalized counts >0 were considered to express the genes.

1299 DVC=dorsal vagal complex; UMAP=uniform manifold approximation and projection; Res.=resolution; GABA=gamma-
1300 aminobutyric acid

1301

1302 Figure 4: *Th* and *Cck* co-expression in the DVC

1303 **A.** UMAP plot of neuronal *Th* and *Cck* scaled expression and cells with co-expression of both
1304 genes (neurons n=48,131; *Th*-expressing neurons n=764; *Cck*-expressing neurons n=3,821;
1305 *Th*/*Cck* co-expressing neurons n=80). On the right plot, cells highlighted in magenta are the co-
1306 expressing neurons. The three neuronal cell identities in which the majority of nuclear co-
1307 expression of *Th* and *Cck* mRNA is found, as well as the percentage of total co-expressing
1308 neurons, are shown. **B.** *In-situ* hybridization of *Cck* and *Th* mRNA in coronal mouse DVC sections
1309 corresponding to -7.2mm and -7.56mm relative to bregma showing overlap of *Th*/*Cck*. Some of
1310 the cells with overlapping signal are highlighted with an arrow in the enhanced merged image.

1311 DVC=dorsal vagal complex; UMAP=uniform manifold approximation and projection

1312

1313 Figure 5: The murine DVC cell hierarchy

1314 **A.** Dendrogram of the harmonized hierarchy which incorporates cells from Ludwig and our
1315 datasets. Orange cell identities are a fourth layer of cell identity resolution obtained as some of
1316 the Ludwig dataset identities are subgroups of our original cell identities at their highest resolution.
1317 Magenta labels represent layer 3 of cellular granularity. These two layers are considered high-

1318 resolution. **B.** UMAP plot of the integration between our and Ludwig datasets using treeArches
1319 (cells n=171,868). **C.** Pairwise heatmap showing the proportion of cells originally labeled in this
1320 study and in Ludwig dataset (y-axis), predicted to belong to each identity group (x-axis) by
1321 treeArches using our learned harmonized hierarchy. In blue are the labels considered non-specific
1322 for a high-resolution cell identity (n=2,324; 1.3%). In pink are the cell labels for rejected cells,
1323 therefore not assigned any identity by treeArches (n=3,108; 1.8%). **D.** UMAP plot of the Dowsett
1324 dataset labeled through treeArches using the learned harmonized hierarchy representation from
1325 our murine DVC atlas. The 'unlabeled' cells include those rejected by the algorithm and thus
1326 without an assigned identity, and those with an unspecific layer-3/4 label. For example, some were
1327 labeled 'neuron' or 'monoamine-class' but without a high-resolution cell identity.
1328 UMAP=uniform manifold approximation and projection; APNTS=Area postrema and nucleus of the solitary tract;
1329 Lnc=long non-coding; OL=oligodendrocyte; OPC=oligodendrocyte precursor cell; Neur=neuronal;
1330 COE=collier/Olf1/EBF transcription factor
1331

1332 <u>Figure 6: The snRNA-seq derived cell identities for the rat DVC</u>
1333 **A.** Schematic of the pipeline for snRNA-seq of the rat DVC. **B.** Labeled UMAP plots of the low
1334 resolution (i.e. layers 1 and 2 of granularity) and **C.** high resolution (i.e. layer 3) cell identities in
1335 our rat DVC dataset (cells n=12,167). We labeled four layer-1, nineteen layer-2 and fifty-two layer-
1336 3 cell identities. Those labels novel to this dataset and not present in the murine data are
1337 highlighted with a pink ♦ symbol. We found a small cluster (cells n=35) that we could not
1338 corroborate its identity at any layer of cellular granularity that we named 'unspecific'.
1339 snRNA-seq=single-nuclei RNA-sequencing; DVC=dorsal vagal complex; FACs=fluorescence-activated cell sorting;
1340 UMAP=uniform manifold approximation and projection; APNTS=Area postrema and nucleus of the solitary tract;
1341 Lnc=long non-coding; OL=oligodendrocyte; OPC=cursor cell; Neur=neuronal; COE=collier/Olf1/EBF transcription
1342 factors
1343

1344 <u>Figure 7: Two novel neuronal classes specific to the rat DVC</u>
1345 **A.** Balloon plots comparing the expression of the marker genes of the two novel neuronal classes
1346 found in rats (cells n=12,167): immunity-akin and the ortus-akin classes (framed in gray).
1347 Expression is shown across the layer-2 rat cell identities. Based on the expression of two DVC
1348 neuronal markers *Mtus2* and *Syt1*, we corroborated those cell classes contain neurons, and not
1349 microglial or vascular/endothelial cells (In orange and red, respectively). The immunity-akin class

1350 (n=48 neurons) shares high expression of *Cst3*, *Inpp5d*, *Csf1r*, *Slco2b1* and *Lyn* with microglial
1351 cells. Meanwhile, the ortus-akin class (n=34 neurons) shows higher overlap of gene expression
1352 markers (i.e. *Arhgap31*, *Pdgfra*, *Bcas1*, *Ppfibp1* and *Itga9*) with OPCs (highlighted with a ♦
1353 symbol). Mouse cell identities (cells n=99,740) do not show these expression patterns (framed in
1354 black). Average expression was calculated using log-normalized counts. **B.** Violin plots of scaled
1355 expression of 10 genes (i.e. *Glp1r, Gfral, Calcr, Ramp3, Gipr, Lepr, Cckar, Cckbr ,Mc4r* and *Prlr*)
1356 coding for metabolism-associated receptors in the Pdgfra and immunity-related rat neurons
1357 (Pdgfra neurons n=34; immunity-related neurons n=48). Pdgfra neurons are the only layer-3
1358 identity within the ortus-akin class. An overlapping dotplot shows one dot per cell. **C.**
1359 Immunofluorescent detection of PDGFRA in mouse and rat DVC. Pink arrowheads point to cells
1360 with OPC morphology, white arrowheads point to cells with fibroblast morphology and the yellow
1361 arrowhead points to cells with neural morphology. **D.** Co-staining for PDGFRA and HuC/D in rat
1362 DVC with high magnification (right images) of area postrema PDGFRA-expressing cells . Yellow
1363 arrowheads indicate colocalization of HuC/D and PDGFRA.
1364 DVC=dorsal vagal complex; OPC=oligodendrocyte precursor cell; AP=area postrema; NTS=nucleus of the solitary
1365 tract; PDGFRA= Platelet-derived growth factor receptor A; CC=central canal
1366

1367 <u>Figure 8: The rodent DVC cell hierarchy</u>
1368 **A.** UMAP plot of the integration between the murine hierarchy and our rat dataset using
1369 treeArches (cells n=184,035). **B.** Dendrogram of the harmonized hierarchy of our labeled rat
1370 dataset and the murine DVC hierarchy. We highlight the incorporated rat cell identities (blue and
1371 magenta). Those in magenta are the novel rat identities established by us. The immunity-akin and
1372 the ortus-akin classes were not found in the murine datasets. The M3 and M5 rat identities are
1373 subgroups of a Ludwig layer 4 cell identity, therefore yields a fifth layer within the monoamine
1374 neuronal class.
1375 UMAP=uniform manifold approximation and projection; DVC=dorsal vagal complex; APNTS=Area postrema and
1376 nucleus of the solitary tract; Lnc=long non-coding; OL=oligodendrocyte; OPC=oligodendrocyte precursor cell;
1377 Neur=neuronal; COE=collier/Olf1/EBF transcription factors
1378

1379 Figure 9: Meal-related transcriptional changes in the mouse DVC

1380 **A.** Horizontal barplots of the number of differential genes between refed and ad libitum fed, and
1381 refed and fasted mice in glial cells and neurons per layer-2 cell identity (MAST algorithm on log-
1382 normalized counts; adj. $p<0.05$; refed neurons n=14,396; refed glial cells n=18,019; ad libitum
1383 fed neurons n= 9,885; ad libitum fed glial cells n=4,610; fasted neurons n=8,829; fasted glial cells
1384 n=12,496). **B.** Venn Diagrams of the differentially expressed genes in magnaclass 1 and
1385 magnaclass 2 neurons between refed and ad libitum fed, and between refed and fasted
1386 treatments (MAST algorithm on log-normalized counts). The number of overlapping log2FC≥1
1387 upregulated genes between the two magnaclasses per treatment are highlighted. The treatment-
1388 induced changes in only one cell class are shown as non-overlapping. The percentage is based
1389 on the total differential genes surveyed per comparison. **C.** Volcano plots of the differential genes
1390 in neurons belonging to the magnaclass 1 and the magnaclass 2 between refed and ad libitum
1391 fed, and **D.** refed and fasted treatments (MAST algorithm on log-normalized counts; adj. $p<0.05$).
1392 Each point represents one gene. Only genes upregulated or downregulated with a log2FC≥2 are
1393 labeled. Since we considered a minimum log fold-change of 0.1 between treatments per cell
1394 group, those genes with very low variance (i.e. log fold-change<0.1) were excluded from the
1395 differential expression analysis, therefore a variable number of genes are shown per comparison
1396 per identity, in the volcano plots.

1397 DVC=dorsal vagal complex; vr=versus; OPC=oligodendrocyte precursor cell; FC=fold-change; adj.=adjusted;
1398 NS=non-significant

1399 Supplementary Material

1400 Figure S1: DVC-centric dissection protocol

1401 **A.** Following euthanasia, the brain is removed from the mouse and briefly rinsed with PBS. To
1402 better visualize the brainstem, the cerebellum is removed with fine forceps. The brain is then
1403 placed within a mouse brain matrix with 1mm spacing between razor guides. In this example
1404 blades will be placed in the 12th (cut 1) and 14th (cut 2) razor guide (these sites are shown).
1405 Using fresh razors make two clean cuts in a single, smooth motion. The bottom showns the
1406 reference images of the mouse brain (from the Allen Brain Institute reference 3D mouse atlas)
1407 visualizing the location of brainstem and the AP/NTS. In these reference images, the cerebellum
1408 is not visualized. **B.** Resultant brainstem tissue from the first two cuts is then further cut twice
1409 more (cuts 3 &4) to keep the middle of the tissue where the DVC is located. This tissue is cut
1410 once more (cut 5) to generate a DVC-centric dissection. Reference images of the mouse brain
1411 (Coronal sections from the Allen Brain Institute reference atlas) displaying the rostral and caudal
1412 sides of tissue collected from cuts 1&2 and the location of cuts 3-5, are shown.

1413

1414 Figure S2: Mapping of *Gad2* and VGLUT2 in neurons

1415 UMAP plot of the murine neurons (n=48,131) showing scaled log-normalized expression of **A.**
1416 *Gad2*, a gene related to GABA synthesis and transmission, **B.** and VGLUT2, a glutamate
1417 transporter. Cells with higher expression of *Gad2* belong to the neuronal magnaclass1, while cells
1418 with higher expression of VGLUT2 (*Slc17a6*) to the magnaclass2 (both highlighted in yellow in
1419 adjacent plots). However, the expression is not mutually exclusive among both classes, nor every
1420 neuron belonging to each class express the respective transcript.

1421 UMAP=uniform manifold approximation and projection; GABA=gamma-aminobutyric acid; VGLUT2=vesicular
1422 glutamate transporter-2

1423

1424 Figure S3: Anatomical mapping of the DVC mouse layer-3 identities

1425 Schematic diagram of the spatial localization for the 35 neuronal identities at layer 3 of resolution
1426 in the mouse DVC. Coronal sections from the mouse brain in the Allen Brain Atlas were used to
1427 manually map the top marker genes of each (MAST algorithm on log-normalized counts; adj.
1428 $p<0.05$) to the DVC.

1429 AP=Area Postrema; NTS= Nucleus of the solitary trac; DMV= Dorsal motor nucleus of the vagus; CC= central canal;
1430 12N= hypoglossal nucleus; Cu=Cuneate nucleus.
1431

1432 Figure S4: Mapping of DVC populations in a murine hypothalamic dataset

1433 UMAP plots of a randomly selected subset of the HypoMap database (cells n=76,260; samples
1434 n=32) labeled **A.** by sample and **B.** by original curated cell class. **C.** Balloon plot showing average
1435 expression of the top 5 upregulated gene markers of each neuronal DVC class (MAST algorithm;
1436 adj. $p<0.05$) in the neurons of the HypoMap subset (n=45,679). We selected the neuronal curated
1437 class cells from our initial HypoMap subset and reprocessed them, including clustering through
1438 *k*-nearest neighbors algorithm using the first 30 PCs and Harmony reduction embeddings.
1439 Resulting clusters at resolution 0.5 are shown. Average expression in the HypoMap neurons was
1440 calculated using log-normalized counts. **D.** Set of UMAP plots showing scaled expression of three
1441 genes (i.e. *Gfap*, *Gria2* and *Kcnj3*) which have a specific pattern of expression in murine DVC
1442 Ca^+-permeable astrocytes. The astrocytic population is circled in purple (astrocytes n=7,629) and
1443 while *Gfap* and *Gria2* expression is in agreement to what we observe in Ca^+-permeable
1444 astrocytes, in the hypothalamic astrocytes *Kcnj3* is not expressed. **E.** Set of UMAP plots of
1445 expression of *Aldh1a1* and *Stk39* which are markers of p-fibroblasts and s-fibroblasts in the DVC.
1446 The hypothalamic fibroblasts are circled in magenta (fibroblasts n=300).
1447 DVC=dorsal vagal complex; UMAP=uniform manifold approximation and projection; AMPAr=α-amino-3-hydroxy-5-
1448 methyl-4-isoxazolepropionic acid receptor; GIRK1=G protein-coupled inwardly rectifying potassium channel 1;
1449 OPC=Oligodendrocyte precursor cell; NG=*Ng2* glial cell
1450

1451 Figure S5: Mapping of DVC Ca^+-permeable astrocytes in other murine brain sites

1452 UMAP plots of a cortical/hippocampal astrocytes dataset by **A.** sample, **B.** brain area and **C.**
1453 original astrocyte type (cell n=1,811). Set of UMAP plots showing scaled expression of three
1454 genes (i.e. *Gfap, Gria2* and *Kcnj3*) which have a specific pattern of expression in murine DVC
1455 Ca^+-permeable astrocytes in **D.** cortical/hippocampal, **E.** forebrain, **F.** pons and **G.** spinal cord
1456 astrocytes. There is some overlap in *Gfap* and *Gria2* expression in cortex, hippocampus and
1457 forebrain, with almost no expression of *Kcnj3*. This is different from what we observe in DVC Ca^+-
1458 permeable astrocytes. In pons and the spinal cord, there is some expression of *Kcnj3*, but the
1459 *Gfap* and *Kcnj3* co-expression is rare.

1460 DVC=dorsal vagal complex; UMAP=uniform manifold approximation and projection
1461

1462 Figure S6: Trajectory inference of the oligodendrocyte lineage

1463 Dotplot of the two principal components obtained through dimensionality reduction using the main
1464 50 principal components analysis on log-normalized gene expression data in oligodendrocytes
1465 (cells n=32,129) **A.** merged and **B.** by sample, and on Harmony embeddings in oligodendrocytes
1466 **C.** merged and **D.** by sample. Cellular trajectory was inferred using SCORPIUS also on normalized
1467 gene expression data (**A.** and **B.**) and on the Harmony embeddings (**C.** and **D.**), and drawn across
1468 the data points (black line). Each data point represents one cell.
1469 OL=oligodendrocyte
1470

1471 Figure S7: Murine DVC clusters

1472 **A.** UMAP plot of the mouse DVC clusters at resolution 1 (cells n=99,740). Cells from mice
1473 exposed to 5 food and aversion-related treatments were integrated using the Harmony algorithm
1474 in R and the resulting embeddings were used to calculate the clusters and UMAP projections. We
1475 subset and re-clustered three clusters containing oligodendrocytes, vascular cells and fibroblasts,
1476 respectively (highlighted). **B.** Violin plots of the two types of fibroblasts in cluster 26, distinguished
1477 by *Skt39* (stress-response 's-fibroblasts') and *Aldh1a1* (perivascular 'p-fibroblasts') expression.
1478 Each data point represents one cell (s-fibroblasts n=244; p-fibroblasts n=559). **C.** UMAP plot of
1479 subclusters from clusters 23 (oligodendrocytes) and **D.** 27 (vascular cells) using the Harmony
1480 embeddings. Gene expression markers for cell populations were mapped (**Table S5**) and the
1481 smallest resolution that allowed to separate them was further used to label the cells. Cells in
1482 subclusters 1 and 2 from cluster 23 were labeled 'premyelinating_OL' whilst subclusters 0 and 3
1483 were labeled 'myelinating_intermediate_OL'. In cluster 27, subcluster 7 was labeled 'pericyte',
1484 subcluster 4 was labeled 'smooth_muscle' and the rest of the clusters were considered to be
1485 endothelial cells.
1486 DVC=dorsal vagal complex; Res.=resolution; UMAP=uniform manifold approximation and projection;
1487 OL=oligodendrocyte; smc=smooth muscle cell.
1488

1489 Figure S8: Mouse microglial activation states

1490 **A.** UMAP plot showing the mapping in the mouse DVC microglia (n=2,787).of monocyte (*Emilin2*
1491 and *Gda*) and microglial (*P2ry12* and *Fcrls*) known differential markers, corroborating the absence
1492 of monocytes in our dataset. **B.** UMAP plot of the microglia from the mouse DVC showing scaled
1493 log-normalized expression of *Cd5*, *Zbp1*, *Cxcl9* and *Cxcl10*. Microglia was subset and re-
1494 processed using the harmony integration embeddings to obtain the UMAP coordinates. **C.** Sub-
1495 clusters at resolution 0.2 of these microglial cells was performed and the **D.** top marker genes are
1496 shown in a balloon plot with average log-normalized counts (MAST algorithm; adj. $p<0.05$) along
1497 with astrocytes and oligodendrocytes (microglia n=2,787, oligodendrocytes n= 32,129,
1498 astrocytes n=11,693). Cluster C3 shares high expression of markers with oligodendrocytes (in
1499 purple) while cluster C5 shares markers with astrocytes (in red). Microglial markers are
1500 highlighted in orange.

1501 UMAP=uniform manifold approximation and projection; DVC=dorsal vagal complex

1502

1503 Figure S9: Mixed neurons sub-clustering

1504 UMAP plots with the mixed neurons of the mouse DVC (mixed neurons n=15,190) showing their
1505 **A.** original layer-3 identity and **B.** final sub-cluster. **C.** Heatmap of the top 5 marker genes (MAST
1506 algorithm; adj. $p<0.05$) expression for each sub-cluster in all neurons (i.e. mixed neurons and all
1507 other neuronal identities, neurons n= 48,131). Each column is one cell and each row is one marker
1508 gene. Some marker genes were duplicated for more than one sub-cluster (e.g. *Nrxn3* is marker
1509 of sub-clusters 2, 3, 8 and 10; *Pcdh9* is marker of sub-clusters 6 and 8) therefore these genes
1510 are only shown once in the plot and highlighted in red.

1511 UMAP=uniform manifold approximation and projection; DVC=dorsal vagal complex

1512

1513 Figure S10: Initial murine cell hierarchy using our samples

1514 **A.** UMAP plot of the integration of our samples (based on the five mouse treatments administered
1515 to mice prior to euthanasia; see **Methods**) using treeArches. There were two cohorts of refed
1516 mice. **B.** UMAP plot of the fifty layer-3 cell identities obtained using the treeArches pipeline. **C.**
1517 Dendrogram showing the initial hierarchy of the three layers of cell identity established by us in
1518 this study.

1519 UMAP=uniform manifold approximation and projection; inj.=injected; APNTS=Area postrema and nucleus of the
1520 solitary tract; Lnc=long non-coding; OL=oligodendrocyte; OPC=oligodendrocyte precursor cell;
1521 COE=collier/Olf1/EBF transcription factors

1522

1523 Figure S11: Incorporation of the Ludwig dataset to our initial hierarchy using treeArches

1524 **A.** Barplot of log-normalized expression of OPC markers (i.e. *Pdgfra*, *Cspg4*, *C1ql1*) and
1525 premyelinating OL markers (i.e. *Bmp4*, *Fyn*) in the OPCs-labeled cells from the Ludwig dataset
1526 (total cells n=1,770; cells expressing >1 marker gene n=1,104). Cells labeled as OPCs in the
1527 Ludwig dataset are a mix of OPC and premyelinating OL. Some cells lack expression of the five
1528 marker genes used in this plot, they are represented on the left side with an empty bar and those
1529 expressing *Fyn*/*Bmp4* but not expressing the OPC markers are likely premyelinating OLs. Cells
1530 were ordered using hierarchical clustering based on these five gene expression data through the
1531 Ward's method in R. We only indicate the 'likely cell identity' for cells with expression of the five
1532 marker genes. **B.** UMAP showing the manual mapping of Ludwig and Dowsett neuronal clusters
1533 and identities in neurons from this study. We used the gene expression markers for all clusters
1534 from Ludwig and Dowsett to identify which of our neurons shared identity with those described in
1535 both publications. Only groups and clusters successfully mapped manually are shown. The
1536 Ludwig identities are in black, Dowsett identities are in blue and our identities are in purple. Most
1537 of neuronal clusters in both publicly available datasets, are subgroups of our cell identities.
1538 OPC=oligodendrocyte precursor cell; OL=oligodendrocyte; UMAP=uniform manifold approximation and projection;
1539 APNTS=Area postrema and nucleus of the solitary tract; Lnc=long non-coding; COE=collier/Olf1/EBF transcription
1540 factors

1541

1542 Figure S12: Rat DVC neurons

1543 **A.** Labeled UMAP plot with the neuronal layer 3 cell identities in our rat dataset (neurons n=4,721).
1544 Neurons were subset and re-processed to obtain the UMAP coordinates. **B.** Violin plots of scaled
1545 expression of 12 genes (i.e. *Gad2, Gad1, Slc6a5, Slc17a7, Slc17a6, Th, Ddc, Nos1, Sst, Npy,*
1546 *Cck* and *Slc5a7*) related to transmission/release of GABA, glutamate, monoamines, nitric oxide,
1547 somatostatin, neuropeptide-Y, cholecystokinin and acetylcholine in the Pdgfra and immunity-
1548 related rat neurons (Pdgfra neurons n=34; immunity-related neurons n=48). An overlapping
1549 dotplot shows one data point representing each cell.

1550 DVC=dorsal vagal complex; UMAP=uniform manifold approximation and projection; COE=collier/Olf1/EBF
1551 transcription factors; Lnc=long non-coding; GABA=gamma-aminobutyric acid
1552

1553 Figure S13: Receptors and neuropeptides expression in mouse and rat neurons

1554 Balloon plot of average nuclear mRNA for a selected list of receptors and neuropeptides related
1555 to metabolism in mouse and rat neurons (rat n= 4,721, mouse n=48,131). Expression values
1556 represent average log-normalized counts for each gene. All cell identities at layer 3 for each
1557 species are shown.
1558

1559 Figure S14: Dendrogram after incorporation of the rat dataset to the murine hierarchy

1560 Dendrogram (i.e. tree) resulting from incorporating our rat dataset (cells n=12,167) to the existing
1561 murine DVC cell hierarchy using treeArches. The rat cell populations in red that did not show
1562 similarity with the previously existing murine identities are appended at the bottom by treeArches
1563 (shown in red).
1564 DVC=dorsal vagal complex
1565

1566 Figure S15: Expression of *Agrp* and *Hcrt* in DVC neurons

1567 **A.** UMAP plots of the neurons (n=48,131) from our murine DVC dataset showing scaled
1568 expression of *Agrp* and *Hcrt*. **B.** *In-situ* hybridization images of *Agrp* and *Hcrt* in the DVC show no
1569 exonic mRNA. We included tissue sections of the arcuate nucleus of the hypothalamus and in the
1570 lateral hypothalamus as controls, and *Agrp* and *Hcrt* were present in these sites, respectively. For
1571 each reaction, tissue from the same mouse was used through two different sections, one including
1572 the DVC and one including the hypothalamic region. **C.** UMAP plots of the Dowsett (n=8,288) and
1573 the Ludwig datasets neurons (n=49,392) showing scaled expression of *Agrp* and *Hcrt*. **D.**
1574 Genome visualization of reads coverage in the *Agrp* and *Hcrt* regions of the *Mus musculus*
1575 refdata-gex-mm10-2020-A reference from two of our mouse sample sequencing replicates.
1576 Resulting BAM files from the original murine DVC FASTQ files were obtained after processing. We
1577 visualized the reads from these BAM files that mapped to the *Agrp* and *Hcrt* genes using IGV
1578 v2.16.1[87]. The coverage of these genes (*Agrp* region: chr8:105,566,180–105,582,268; *Hcrt*
1579 region: chr11:100,761,693–100,762,931) are shown in gray. The majority of the reads mapped
1580 to the intronic regions of *Agrp*, and to the last part of the 3'-end of exon 2 and the 3'-untranslated

1581 region of *Hcrt*. **E.** UMAP plot of rat DVC neurons (n=4,721) showing scaled expression of *Agrp*
1582 and *Hcrt*. For all UMAP projections, neurons from each dataset were subset based on our labeling
1583 for our murine and rat datasets, the treeArches resulting labeling for the Dowsett dataset, and the
1584 original labeling from Ludwig and collaborators. Then the neurons were processed using
1585 Seurat[23] and integrated using Harmony[25], to yield the final UMAP embeddings.
1586 DVC=dorsal vagal complex; UMAP=uniform manifold approximation and projection; AP=area postrema;
1587 NTS=nucleus of the solitary tract; ARH=arcuate nucleus of the hypothalamus; 3v=third ventricle; ME=median
1588 eminence; LH=lateral hypothalamus. BAM=binary alignment map
1589

1590 Figure S16: Expression of metabolism-associated receptors in the DVC magnaclasses
1591 Violin plots of scaled expression of 10 genes (i.e. *Glp1r, Gfral, Calcr, Ramp3, Gipr, Lepr, Cckar,*
1592 *Cckbr ,Mc4r* and *Prlr*) coding for metabolism-associated receptors in the magnaclass1 and
1593 magnaclass2 neurons of the mouse DVC in fasted (magnaclass1 n=2,756; magnaclass2
1594 n=2,789) and refed (magnaclass1 n=4,586; magnaclass2 n=4,423).
1595 DVC=dorsal vagal complex
1596

1597 Table S1: Filtering of our and Dowsett datasets during processing
1598 Compilation of statistics and cells processed for the initial high quality cell filtering per sample.
1599

1600 Table S2: Cluster filtering of our and Dowsett datasets during processing
1601 Compilation of low quality cluster analysis statistics to filter high quality clusters per sample.
1602

1603 Table S3: Singlets retained per dataset after processing
1604 Number of doublets and singlets identified by DoubletFinder[24] after initial filtering of our and
1605 Dowset dataset per sample. Doublets were removed from the datasets before sample integration
1606 with Harmony[25] (this step was not performed in the rat dataset as it was only one sample, n=2
1607 rat DVC).
1608

1609 Table S4: Murine brain databases used to map our unlabeled mouse dataset
1610 We used four databases included in the scRNAseq v2.16.0[26-28, 31, 55] R package and the
1611 celldex v1.12.0 built-in mouse RNA-seq reference (which we called 'SingleR' database) using

1612 SingleR [30] function to transfer labels to our dataset in R[22]. The name, brain area and
1613 reference in which each database was made public are specified.
1614
1615 Table S5: Literature-derived markers per central nervous system cell identity
1616 We thoroughly searched in the literature for established markers at the mRNA and/or protein level.
1617 Some markers were found to be described for more than one cell population which are specified
1618 in columns 'notes' and 'notes_2'. After initial labeling of our murine dataset with the databases as
1619 described, we proceeded to obtain the average expression (on log-normalized counts) of each
1620 gene coding for the markers for the labeled cells (i.e. astrocyte, endothelial, microglia, neuron and
1621 oligodendrocyte) and unlabeled cells (i.e. unknown). We also calculated the average expression
1622 for each cluster in our dataset, established during our processing pipeline, at resolution 1.0.
1623
1624 Table S6: Description of our DVC layer-3 neuronal cell identities established in mice
1625 Neurons were subset and reprocessed before labeling at layer-3 granularity. The MAST
1626 algorithm[32] was used through Seurat v5[23]on scaled data with a log fold-change threshold of
1627 0.25 and detection threshold on ≥40% of cells on each neuronal cluster at resolution 1.0. We
1628 searched the resulting gene expression markers in the literature and compiled them. We then
1629 based the names for our cell identities on these genes.
1630
1631 Table S7: Literature-derived markers per central nervous system cell identity
1632 Breakdown of the cell identities (except neurons at layer 3 of cellular resolution) we established
1633 and corroborating using a combination of markers surveyed in **Table S2** and additional markers
1634 established using the FindConservedMarkers function from Seurat v5[23] package, indicating a
1635 cell state derived from the literature. For example, 's_fibroblasts' were named after finding high
1636 expression of *Stk39*, a stress-related marker[56].
1637
1638 Table S8: Expression of the murine DVC identity markers by rat DVC clusters
1639 Average log-normalized expression of the top 5 gene expression markers of each of our murine
1640 layer-3 cell identities (except duplicated genes n=37, and mouse specific genes n=27; total genes
1641 included=186) by rat DVC cluster at resolution 2.0.

1642

1643 Table S9: Description of our DVC layer-3 neuronal cell identities established in rats

1644 Rat neurons were subset and reprocessed before labeling at layers 2 and 3 of granularity. We
1645 used neuronal class gene expression markers to identify clusters at resolution 2.0 that belonged
1646 to each neuronal cell class. These cell classes were further subclustered and markers from Table
1647 S6 and UMAP projections were used to label each population in the dataset.

1648

1649 Table S10: Labeled cells in our murine dataset

1650 Number of cell per treatment per identity layer 2.

1651

1652 Table S11: Expression of neurotransmitter-related genes in our murine neurons

1653 Expression of genes coding for neurotransmitter synthesis enzymes TH, DBH, TPH, GABA, NOS,
1654 prohormone SST and primary neurotransmitter transporters VMAT2, VGLUT1, VGLUT2, GLYT2
1655 per neuron in our dataset. Expression and glutamate and GABA release are specified as binary
1656 variables (i.e. 0=no expression; 1=expression) in the green and blue columns, respectively. The
1657 percentile of the log-normalized expression is shown. ~55% of the neurons display expression of
1658 genes related to the synthesis/release of >1 primary neurotransmitter.

1659

1660 Table S12: Receptor expression in magnaclasses 1 and 2 between meal-related treatments in
1661 mice

1662 Differential expression analysis (MAST algorithm)[32] results for genes coding for metabolism
1663 related receptors between meal-related treatments (i.e. refed versus ad libitum fed, and refed
1664 versus overnight fasted) and per neuronal magnaclass. If a receptor is missing for any given
1665 comparison for any of the magnaclasses, the log fold-change of that gene between both
1666 treatments in that neuronal class was <0.1, therefore it is not reported (see **Methods**).

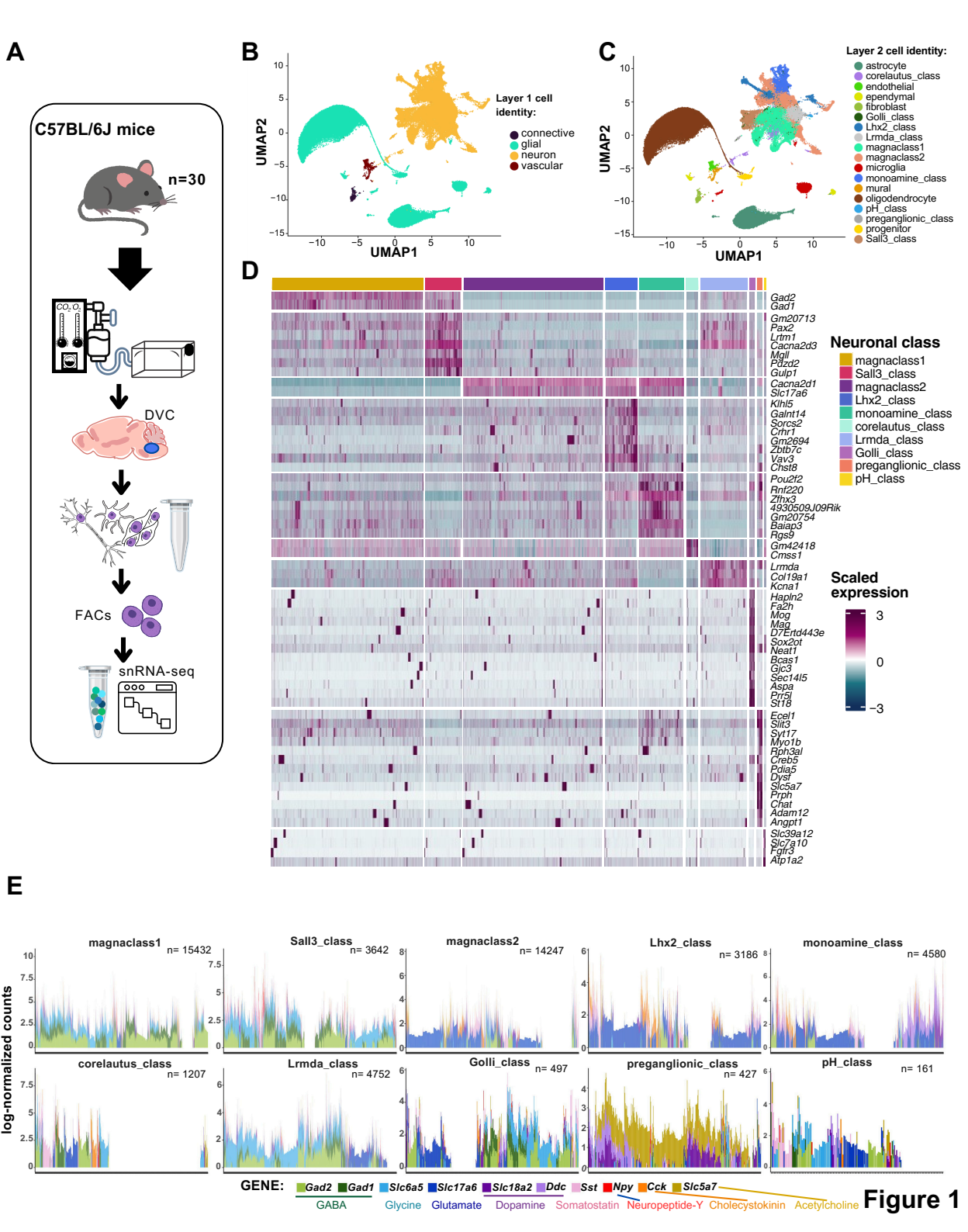
A
C57BL/6J mice
n=30
DVC
FACs
snRNA-seq
B
UMAP2
UMAP1
Layer 1 cell identity:
connective
glial
neuron
vascular
C
Layer 2 cell identity:
astrocyte
corelautus_class
endothelial
ependymal
fibroblast
Golli_class
Lhx2_class
Lrmda_class
magnaclass1
magnaclass2
microglia
monoamine_class
mural
oligodendrocyte
pH_class
preganglionic_class
progenitor
Sall3_class
D
Neuronal class
magnaclass1
Sall3_class
magnaclass2
Lhx2_class
monoamine_class
corelautus_class
Lrmda_class
Golli_class
preganglionic_class
pH_class
Scaled expression
Gad2
Gad1
Gm20713
Pax2
Lrtm1
Cacna2d3
Mgll
Pdzd2
Gulp1
Cacna2d1
Slc17a6
Klhl5
Galnt14
Sorcs2
Crhr1
Gm2694
Zbtb7c
Vav3
Chst8
Pou2f2
Rnf220
Zfhx3
4930509J09Rik
Gm20754
Baiap3
Rgs9
Gm42418
Cmss1
Lrmda
Col19a1
Kcna1
Hapln2
Fa2h
Mog
Mag
D7Ertd443e
Sox2ot
Neat1
Bcas1
Gjc3
Sec14l5
Aspa
Prrg1
St18
Ecel1
Slit3
Syt17
Myo1b
Rph3al
Creb5
Pdia5
Dyst
Slc5a7
Prph
Chat
Adam12
Angpt1
Slc39a12
Slc7a10
Fgfr3
Atp1a2
E
log-normalized counts
magnaclass1 n= 15432
Sall3_class n= 3642
magnaclass2 n= 14247
Lhx2_class n= 3186
monoamine_class n= 4580
corelautus_class n= 1207
Lrmda_class n= 4752
Golli_class n= 497
preganglionic_class n= 427
pH_class n= 161
GENE:
Gad2 Gad1 Slc6a5 Slc17a6 Slc18a2 Ddc Sst Npy Cck Slc5a7
GABA Glycine Glutamate Dopamine Somatostatin Neuropeptide-Y Cholecystokinin Acetylcholine

Figure 1

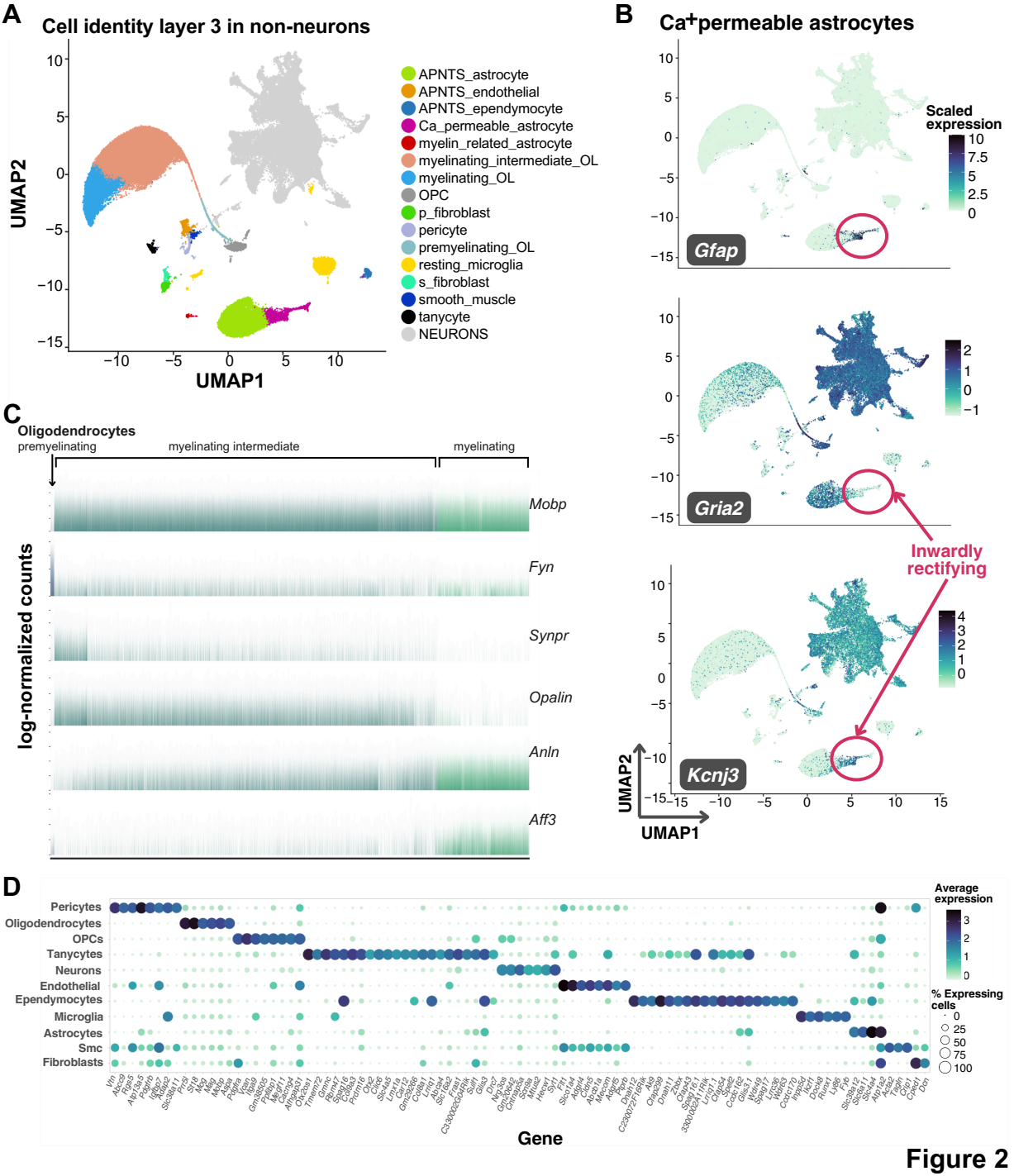
A
Cell identity layer 3 in non-neurons
UMAP2
UMAP1
APNTS_astrocyte
APNTS_endothelial
APNTS_ependymocyte
Ca_permeable_astrocyte
myelin_related_astrocyte
myelinating_intermediate_OL
myelinating_OL
OPC
p_fibroblast
pericyte
premyelinating_OL
resting_microglia
s_fibroblast
smooth_muscle
tanycyte
NEURONS
B
Ca+permeable astrocytes
Scaled expression
Gfap
Gria2
Kcnj3
Inwardly rectifying
UMAP2
UMAP1
C
Oligodendrocytes
premyelinating
myelinating intermediate
myelinating
log-normalized counts
Mobp
Fyn
Synpr
Opalin
Anln
Aff3
D
Pericytes
Oligodendrocytes
OPCs
Tanycytes
Neurons
Endothelial
Ependymocytes
Microglia
Astrocytes
Smc
Fibroblasts
Average expression
% Expressing cells
Gene

Figure 2

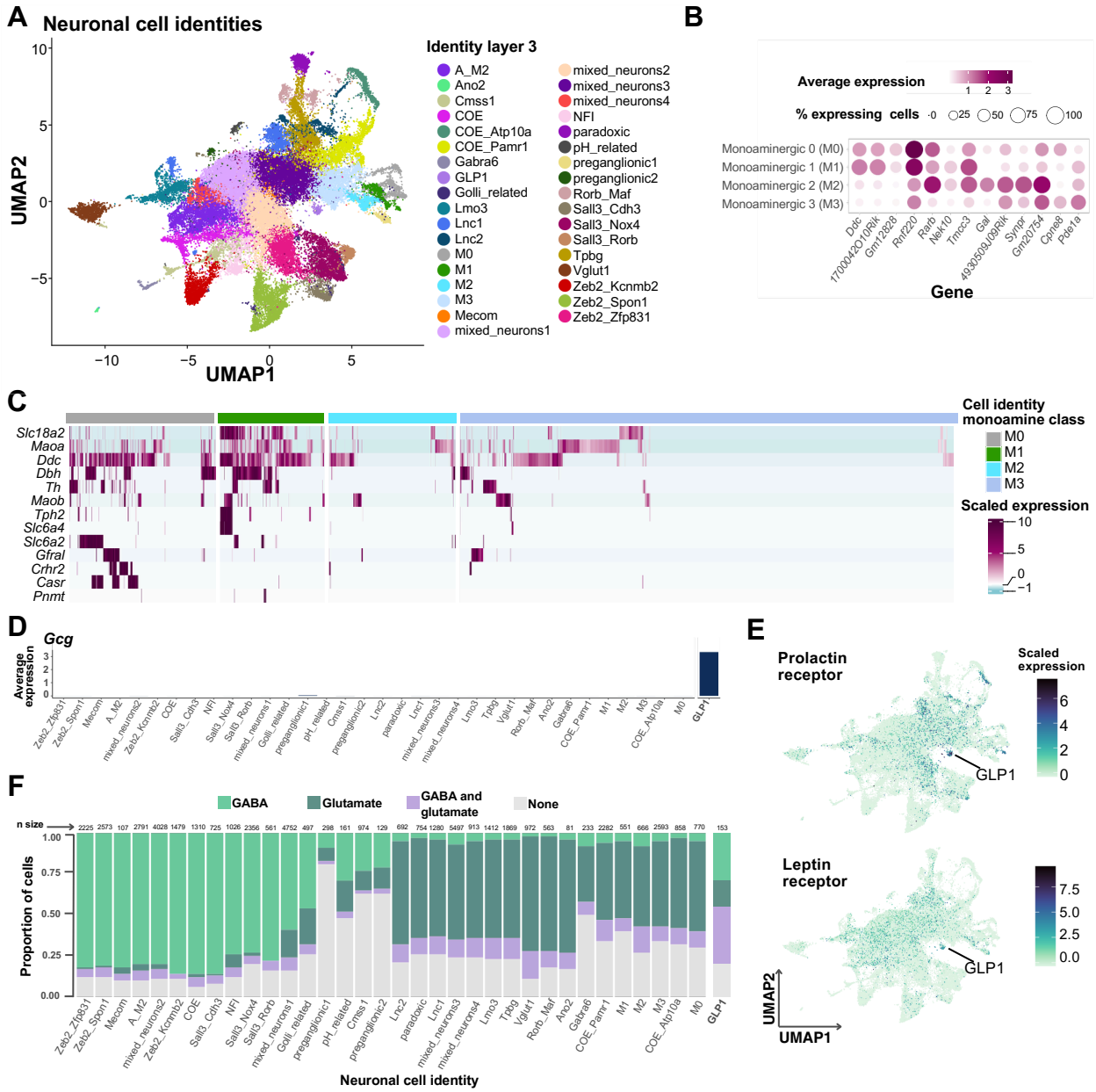
A
Neuronal cell identities
UMAP2
UMAP1
Identity layer 3
A_M2
Ano2
Cmss1
COE
COE_Atp10a
COE_Pamr1
Gabra6
GLP1
Golli_related
Lmo3
Lnc1
Lnc2
M0
M1
M2
M3
Mecom
mixed_neurons1
mixed_neurons2
mixed_neurons3
mixed_neurons4
NFI
paradoxic
pH_related
preganglionic1
preganglionic2
Rorb_Maf
Sall3_Cdh3
Sall3_Nox4
Sall3_Rorb
Tpbg
Vglut1
Zeb2_Kcnmb2
Zeb2_Spon1
Zeb2_Zfp831
B
Average expression
% expressing cells
Monoaminergic 0 (M0)
Monoaminergic 1 (M1)
Monoaminergic 2 (M2)
Monoaminergic 3 (M3)
Ddc
1700042O10Rik
Gm12928
Rnf220
Rarb
Nek10
Tmcc3
Gal
4930503J09Rik
Syngr
Gm20754
Cpne8
Pde1a
Gene
C
Slc18a2
Maoa
Ddc
Dbh
Th
Maob
Tph2
Slc6a4
Slc6a2
Gfral
Crhr2
Casr
Pnmt
Cell identity monoamine class
M0
M1
M2
M3
Scaled expression
D
Gcg
Average expression
E
Prolactin receptor
Leptin receptor
Scaled expression
GLP1
UMAP2
UMAP1
F
GABA
Glutamate
GABA and glutamate
None
n size
Proportion of cells
Neuronal cell identity

Figure 3

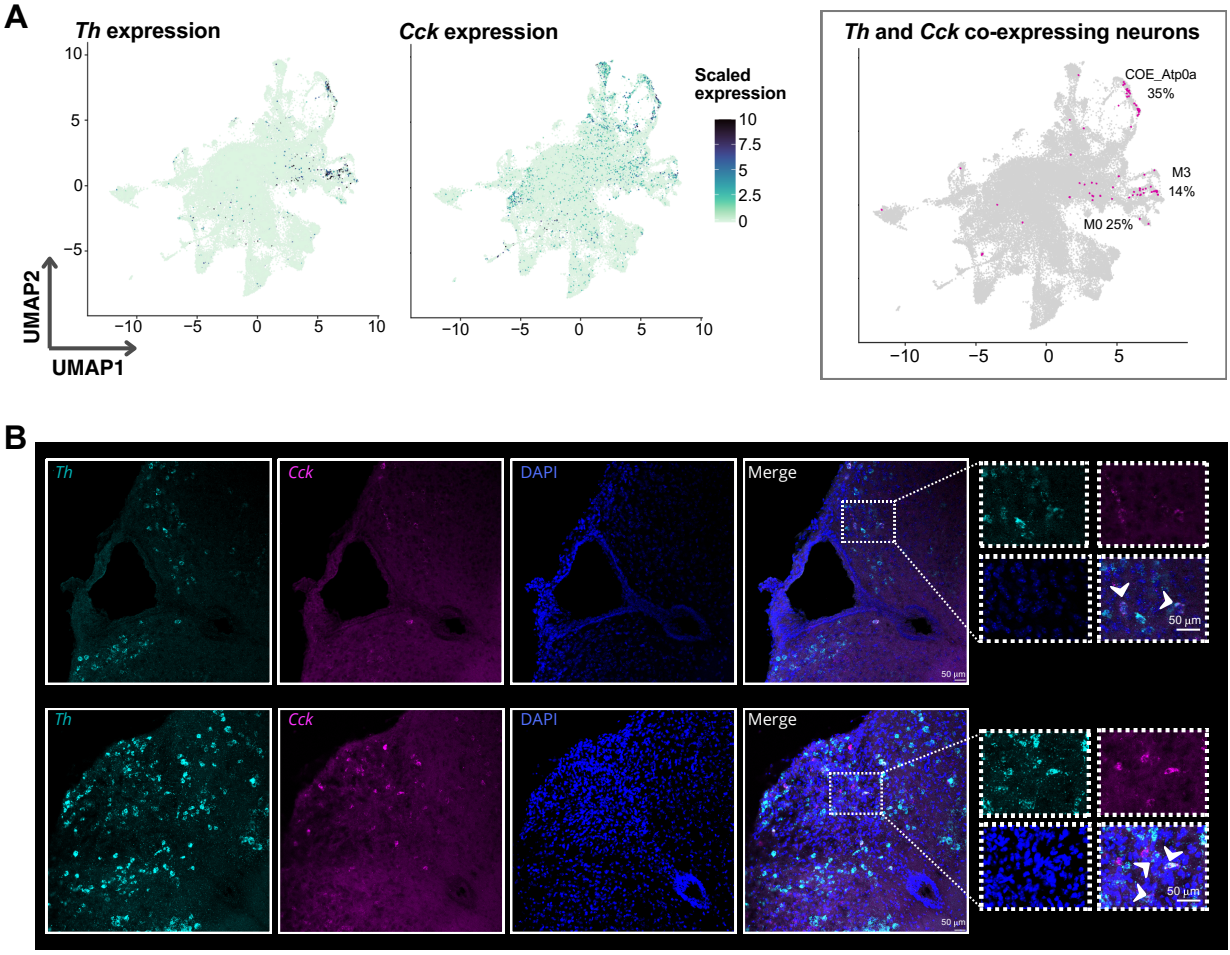
A
Th expression
Cck expression
Scaled expression
10
7.5
5
2.5
0
UMAP2
UMAP1
Th and Cck co-expressing neurons
COE_Atp0a
35%
M3
14%
M0 25%
B
Th
Cck
DAPI
Merge
50 µm

Figure 4

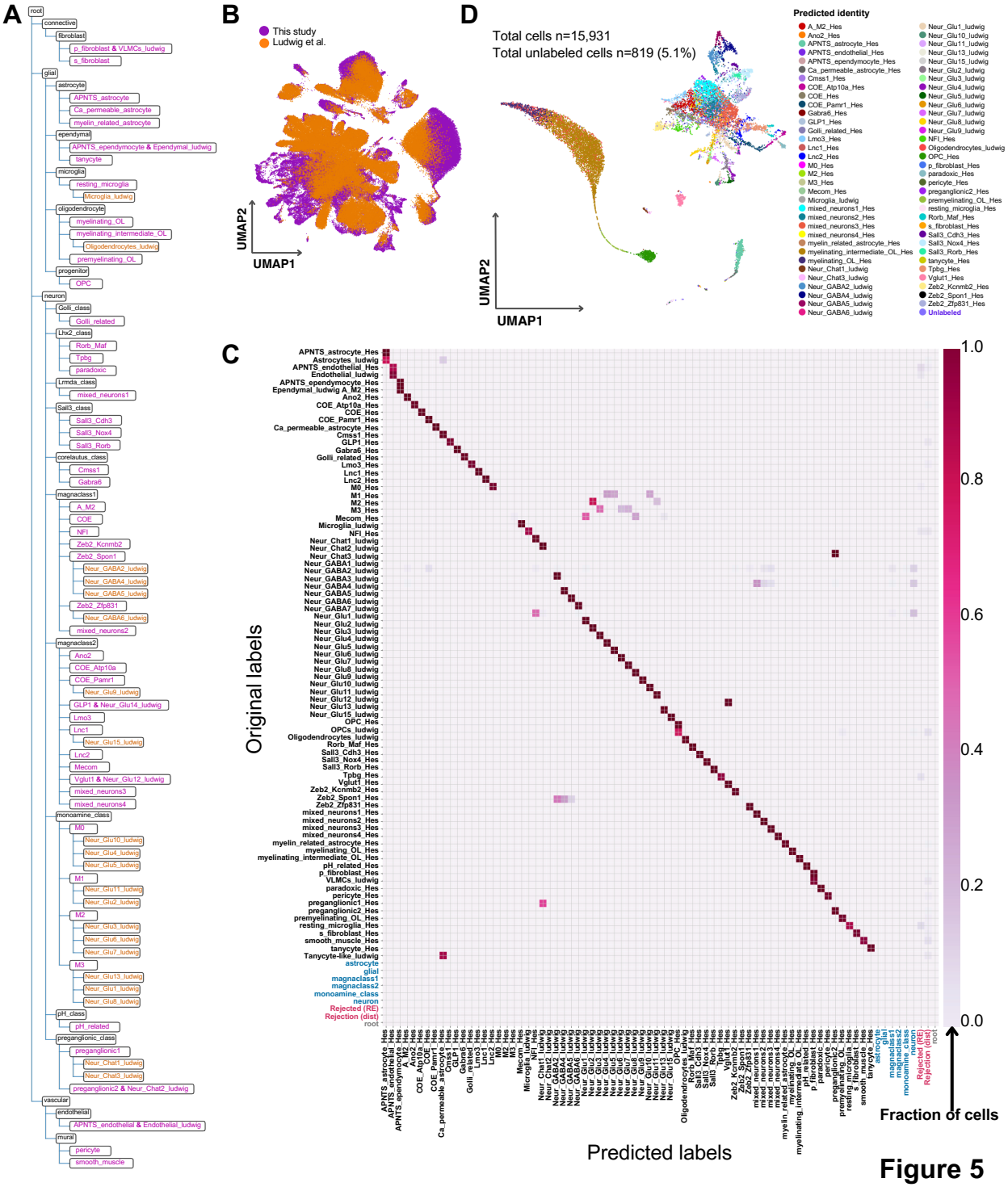
A
root
connective
fibroblast
p_fibroblast & VLMCs_ludwig
s_fibroblast
glial
astrocyte
APNTS_astrocyte
Ca_permeable_astrocyte
myelin_related_astrocyte
ependymal
APNTS_ependymocyte & Ependymal_ludwig
tanycyte
microglia
resting_microglia
Microglia_ludwig
oligodendrocyte
myelinating_OL
myelinating_intermediate_OL
Oligodendrocytes_ludwig
premyelinating_OL
progenitor
OPC
neuron
Golli_class
Golli_related
Lhx2_class
Rorb_Maf
Tpbg
paradoxic
Lrmda_class
mixed_neurons1
Sall3_class
Sall3_Cdh3
Sall3_Nox4
Sall3_Rorb
corelautus_class
Cmss1
Gabra6
magnaclass1
A_M2
COE
NFI
Zeb2_Kcnmb2
Zeb2_Spon1
Neur_GABA2_ludwig
Neur_GABA4_ludwig
Neur_GABA5_ludwig
Zeb2_Zfp831
Neur_GABA6_ludwig
mixed_neurons2
magnaclass2
Ano2
COE_Atp10a
COE_Pamr1
Neur_Glu9_ludwig
GLP1 & Neur_Glu14_ludwig
Lmo3
Lnc1
Neur_Glu15_ludwig
Lnc2
Mecom
Vglut1 & Neur_Glu12_ludwig
mixed_neurons3
mixed_neurons4
monoamine_class
M0
Neur_Glu10_ludwig
Neur_Glu4_ludwig
Neur_Glu5_ludwig
M1
Neur_Glu11_ludwig
Neur_Glu2_ludwig
M2
Neur_Glu3_ludwig
Neur_Glu6_ludwig
Neur_Glu7_ludwig
M3
Neur_Glu13_ludwig
Neur_Glu1_ludwig
Neur_Glu8_ludwig
pH_class
pH_related
preganglionic_class
preganglionic1
Neur_Chat1_ludwig
Neur_Chat3_ludwig
preganglionic2 & Neur_Chat2_ludwig
vascular
endothelial
APNTS_endothelial & Endothelial_ludwig
mural
pericyte
smooth_muscle
B
This study
Ludwig et al.
UMAP2
UMAP1
D
Total cells n=15,931
Total unlabeled cells n=819 (5.1%)
UMAP2
UMAP1
Predicted identity
A_M2_Hes
Ano2_Hes
APNTS_astrocyte_Hes
APNTS_endothelial_Hes
APNTS_ependymocyte_Hes
Ca_permeable_astrocyte_Hes
Cmss1_Hes
COE_Atp10a_Hes
COE_Hes
COE_Pamr1_Hes
Gabra6_Hes
GLP1_Hes
Golli_related_Hes
Lmo3_Hes
Lnc1_Hes
Lnc2_Hes
M0_Hes
M1_Hes
M2_Hes
M3_Hes
Mecom_Hes
Microglia_ludwig
mixed_neurons1_Hes
mixed_neurons2_Hes
mixed_neurons3_Hes
mixed_neurons4_Hes
myelin_related_astrocyte_Hes
myelinating_intermediate_OL_Hes
myelinating_OL_Hes
Neur_Chat1_ludwig
Neur_Chat3_ludwig
Neur_GABA2_ludwig
Neur_GABA4_ludwig
Neur_GABA5_ludwig
Neur_GABA6_ludwig
Neur_Glu1_ludwig
Neur_Glu2_ludwig
Neur_Glu3_ludwig
Neur_Glu4_ludwig
Neur_Glu5_ludwig
Neur_Glu6_ludwig
Neur_Glu7_ludwig
Neur_Glu8_ludwig
Neur_Glu9_ludwig
NFI_Hes
Oligodendrocytes_ludwig
OPC_Hes
p_fibroblast_Hes
paradoxic_Hes
pericyte_Hes
preganglionic2_Hes
premyelinating_OL_Hes
resting_microglia_Hes
Rorb_Maf_Hes
s_fibroblast_Hes
Sall3_Cdh3_Hes
Sall3_Nox4_Hes
Sall3_Rorb_Hes
tanycyte_Hes
Tpbg_Hes
Vglut1_Hes
Zeb2_Kcnmb2_Hes
Zeb2_Spon1_Hes
Zeb2_Zfp831_Hes
Unlabeled
C
Original labels
Predicted labels
Fraction of cells
1.0
0.8
0.6
0.4
0.2
0.0

Figure 5

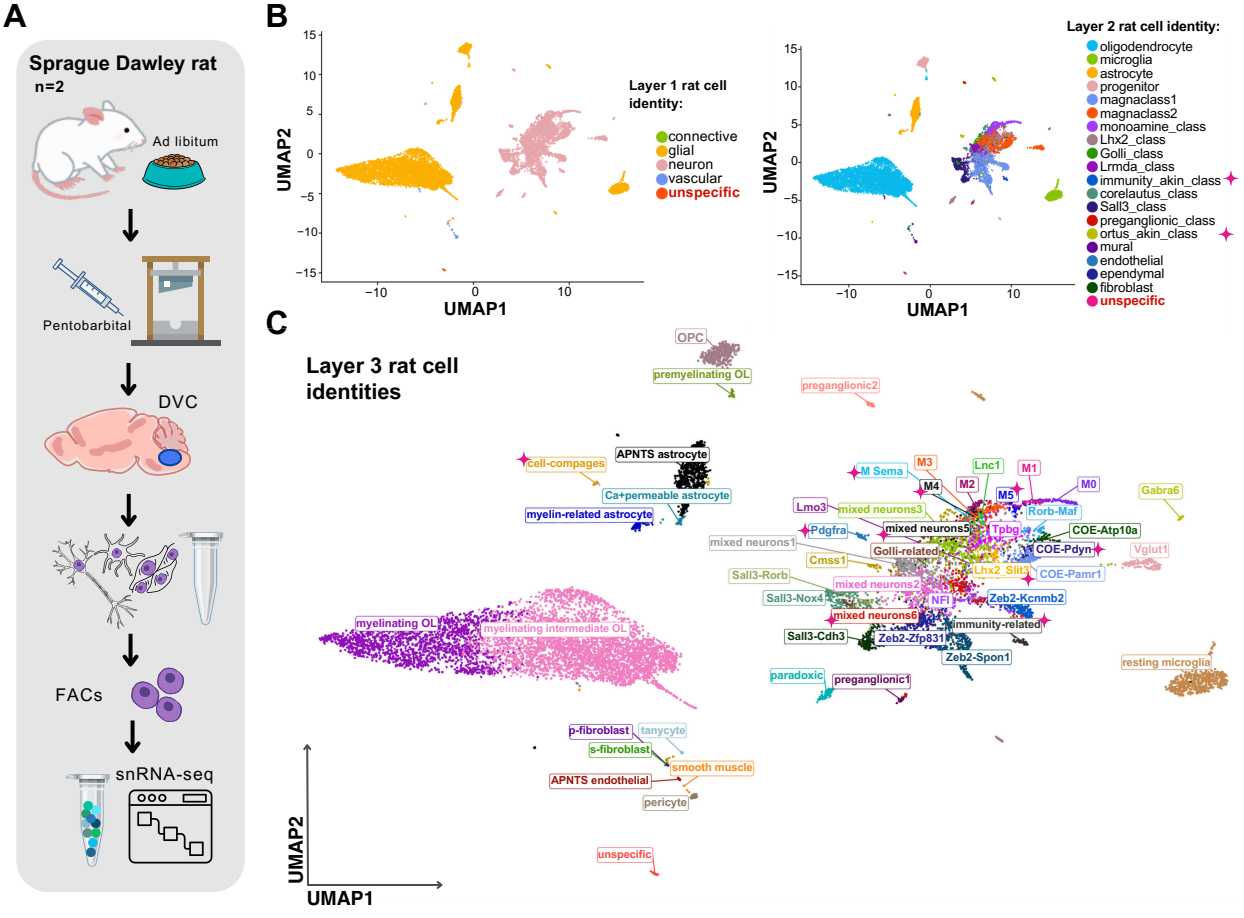
A
Sprague Dawley rat
n=2
Ad libitum
Pentobarbital
DVC
FACs
snRNA-seq
B
UMAP2
UMAP1
Layer 1 rat cell identity:
connective
glial
neuron
vascular
unspecific
Layer 2 rat cell identity:
oligodendrocyte
microglia
astrocyte
progenitor
magnaclass1
magnaclass2
monoamine_class
Lhx2_class
Golli_class
Lrmda_class
immunity_akin_class
corelautus_class
Sall3_class
preganglionic_class
ortus_akin_class
mural
endothelial
ependymal
fibroblast
unspecific
C
Layer 3 rat cell identities
OPC
premyelinating OL
preganglionic2
cell-compages
APNTS astrocyte
Ca+permeable astrocyte
myelin-related astrocyte
M Sema
M3
Lnc1
M1
M4
M2
M5
M0
Gabra6
Lmo3
mixed neurons3
Rorb-Maf
Pdgfra
mixed neurons5
Tpbg
COE-Atp10a
mixed neurons1
Golli-related
COE-Pdyn
Vglut1
Cmss1
Lhx2_Slit3
COE-Pamr1
Sall3-Rorb
mixed neurons2
Sall3-Nox4
NFI
Zeb2-Kcnmb2
mixed neurons6
immunity-related
Sall3-Cdh3
Zeb2-Zfp831
Zeb2-Spon1
resting microglia
paradoxic
preganglionic1
myelinating OL
myelinating intermediate OL
p-fibroblast
tanycyte
s-fibroblast
smooth muscle
APNTS endothelial
pericyte
unspecific
UMAP2
UMAP1

Figure 6

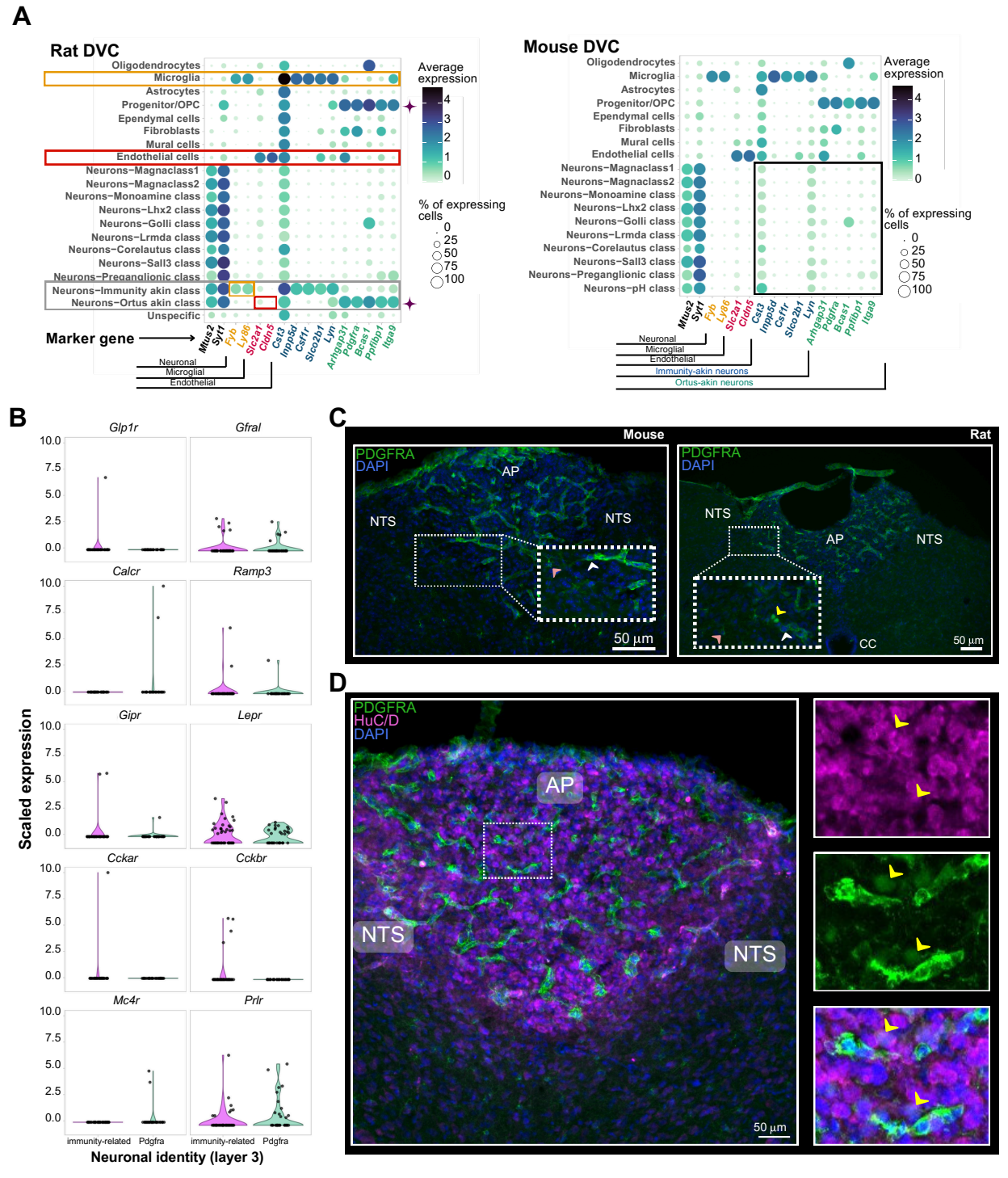
A
Rat DVC
Mouse DVC
Oligodendrocytes
Microglia
Astrocytes
Progenitor/OPC
Ependymal cells
Fibroblasts
Mural cells
Endothelial cells
Neurons−Magnaclass1
Neurons−Magnaclass2
Neurons−Monoamine class
Neurons−Lhx2 class
Neurons−Golli class
Neurons−Lrmda class
Neurons−Corelautus class
Neurons−Sall3 class
Neurons−Preganglionic class
Neurons−Immunity akin class
Neurons−Ortus akin class
Neurons−pH class
Unspecific
Average expression
% of expressing cells
Marker gene
Mtus2
Syt1
Fyb
Lyl6
Slc2a1
Cldn5
Cst3
Inpp5d
Csf1r
Slco2b1
Lyn
Arhgap31
Pdgfra
Bcas1
Ppfibp1
Itga9
Neuronal
Microglial
Endothelial
Immunity-akin neurons
Ortus-akin neurons
B
Glp1r
Gfral
Calcr
Ramp3
Gipr
Lepr
Cckar
Cckbr
Mc4r
Prlr
Scaled expression
immunity-related
Pdgfra
Neuronal identity (layer 3)
C
Mouse
Rat
PDGFRA
DAPI
AP
NTS
CC
50 µm
D
HuC/D

Figure 7

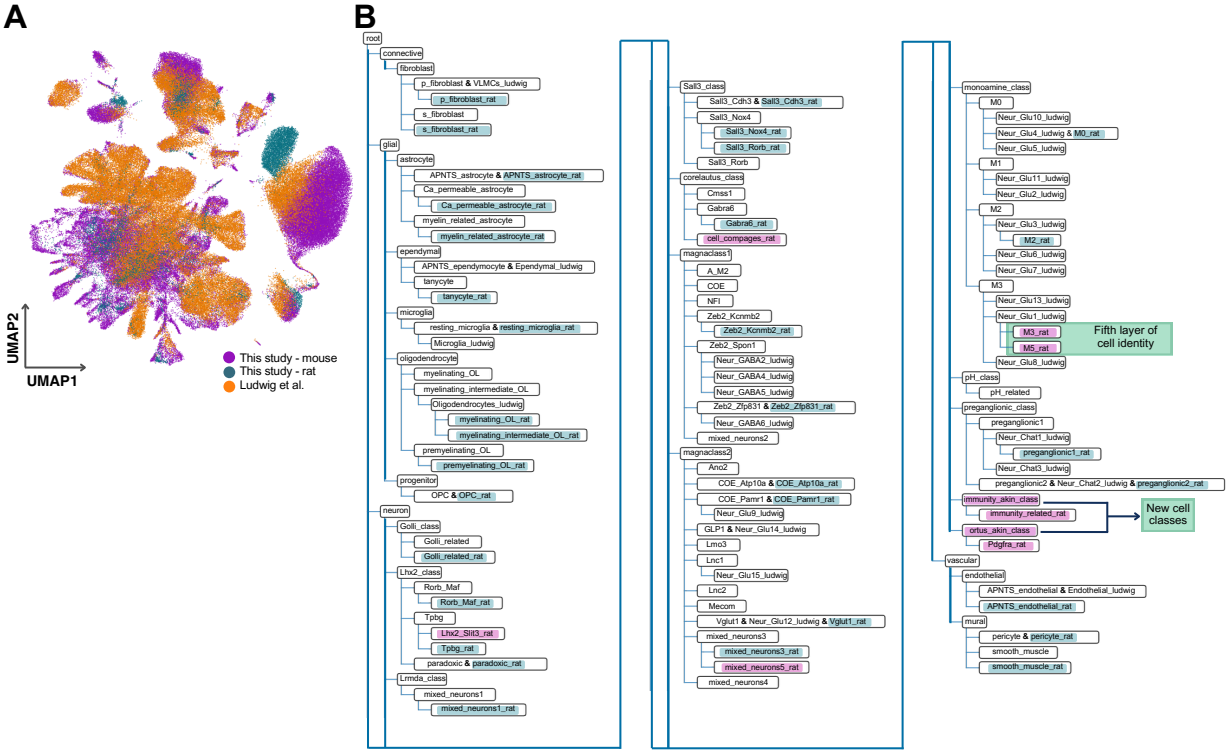
A
UMAP2
UMAP1
This study - mouse
This study - rat
Ludwig et al.
B
root
connective
fibroblast
p_fibroblast & VLMCs_ludwig
p_fibroblast_rat
s_fibroblast
s_fibroblast_rat
glial
astrocyte
APNTS_astrocyte & APNTS_astrocyte_rat
Ca_permeable_astrocyte
Ca_permeable_astrocyte_rat
myelin_related_astrocyte
myelin_related_astrocyte_rat
ependymal
APNTS_ependymocyte & Ependymal_ludwig
tanycyte
tanycyte_rat
microglia
resting_microglia & resting_microglia_rat
Microglia_ludwig
oligodendrocyte
myelinating_OL
myelinating_intermediate_OL
Oligodendrocytes_ludwig
myelinating_OL_rat
myelinating_intermediate_OL_rat
premyelinating_OL
premyelinating_OL_rat
progenitor
OPC & OPC_rat
neuron
Golli_class
Golli_related
Golli_related_rat
Lhx2_class
Rorb_Maf
Rorb_Maf_rat
Tpbg
Lhx2_Sitl3_rat
Tpbg_rat
paradoxic & paradoxic_rat
Lrmda_class
mixed_neurons1
mixed_neurons1_rat
Sall3_class
Sall3_Cdh3 & Sall3_Cdh3_rat
Sall3_Nox4
Sall3_Nox4_rat
Sall3_Rorb_rat
Sall3_Rorb
corelautus_class
Cmss1
Gabra6
Gabra6_rat
cell_compages_rat
magnaclass1
A_M2
COE
NF1
Zeb2_Kcnmb2
Zeb2_Kcnmb2_rat
Zeb2_Spon1
Neur_GABA2_ludwig
Neur_GABA4_ludwig
Neur_GABA5_ludwig
Zeb2_Zfp831 & Zeb2_Zfp831_rat
Neur_GABA6_ludwig
mixed_neurons2
magnaclass2
Anc2
COE_Atp10a & COE_Atp10a_rat
COE_Pamr1 & COE_Pamr1_rat
Neur_Glu9_ludwig
GLP1 & Neur_Glu14_ludwig
Lmo3
Lnc1
Neur_Glu15_ludwig
Lnc2
Mecom
Vglut1 & Neur_Glu12_ludwig & Vglut1_rat
mixed_neurons3
mixed_neurons3_rat
mixed_neurons5_rat
mixed_neurons4
monoamine_class
M0
Neur_Glu10_ludwig
Neur_Glu4_ludwig & M0_rat
Neur_Glu5_ludwig
M1
Neur_Glu11_ludwig
Neur_Glu2_ludwig
M2
Neur_Glu3_ludwig
M2_rat
Neur_Glu6_ludwig
Neur_Glu7_ludwig
M3
Neur_Glu13_ludwig
Neur_Glu1_ludwig
M3_rat
M5_rat
Fifth layer of cell identity
Neur_Glu8_ludwig
pH_class
pH_related
preganglionic_class
preganglionic1
Neur_Chat1_ludwig
preganglionic1_rat
Neur_Chat3_ludwig
preganglionic2 & Neur_Chat2_ludwig & preganglionic2_rat
immunity_akin_class
immunity_related_rat
ortus_akin_class
Pdgfra_rat
New cell classes
vascular
endothelial
APNTS_endothelial & Endothelial_ludwig
APNTS_endothelial_rat
mural
pericyte & pericyte_rat
smooth_muscle
smooth_muscle_rat

Figure 8

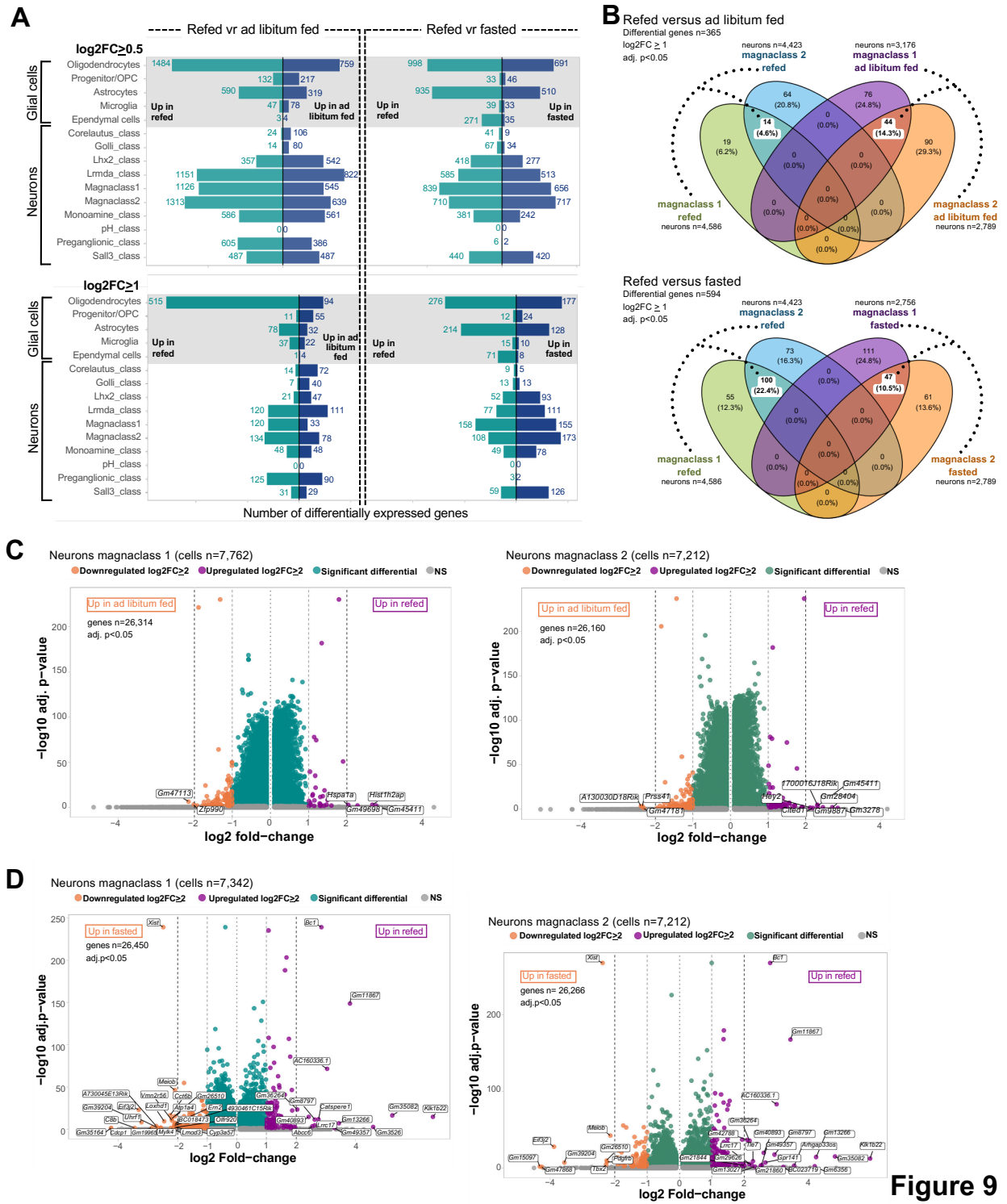
A
Refed vr ad libitum fed
Refed vr fasted
log2FC≥0.5
Glial cells
Neurons
Oligodendrocytes
Progenitor/OPC
Astrocytes
Microglia
Ependymal cells
Corelautus_class
Golli_class
Lhx2_class
Lrmda_class
Magnaclass1
Magnaclass2
Monoamine_class
pH_class
Preganglionic_class
Sall3_class
Up in refed
Up in ad libitum fed
Up in refed
Up in fasted
log2FC≥1
Up in refed
Up in ad libitum fed
Up in refed
Up in fasted
Number of differentially expressed genes
B
Refed versus ad libitum fed
Differential genes n=365
log2FC ≥ 1
adj. p<0.05
neurons n=4,423
magnaclass 2
refed
neurons n=3,176
magnaclass 1
ad libitum fed
magnaclass 1
refed
neurons n=4,586
magnaclass 2
ad libitum fed
neurons n=2,789
Refed versus fasted
Differential genes n=594
log2FC ≥ 1
adj. p<0.05
neurons n=4,423
magnaclass 2
refed
neurons n=2,756
magnaclass 1
fasted
magnaclass 1
refed
neurons n=4,586
magnaclass 2
fasted
neurons n=2,789
C
Neurons magnaclass 1 (cells n=7,762)
Downregulated log2FC≥2
Upregulated log2FC≥2
Significant differential
NS
Up in ad libitum fed
genes n=26,314
adj. p<0.05
Up in refed
−log10 adj. p−value
log2 fold−change
Neurons magnaclass 2 (cells n=7,212)
Up in ad libitum fed
genes n=26,160
adj. p<0.05
Up in refed
D
Neurons magnaclass 1 (cells n=7,342)
Up in fasted
genes n=26,450
adj.p<0.05
Up in refed
−log10 adj.p−value
log2 Fold−change
Neurons magnaclass 2 (cells n=7,212)
Up in fasted
genes n= 26,266
adj.p<0.05
Up in refed
−log10 adj.p−value
log2 Fold−change

Figure 9